Table 1: Summary of Glycosylation Analysis of IgLON Family Proteins

protein	peptides		glycopeptides							*N*-glycan				
										deduced monosaccharide composition				
		sequence[a,b]	elution position	Figure	peak no.[c]	scan in Figure 4A[d]	observed peptide-related ion[e]	observed *m/z* in SIM mode[b]	theoretical *m/z*[b]	dHex	Hex	HexNAc	NA	deduced structure[f] (diagnostic ion)
LAMP	B	GTDN[12]ITVR (874.451)	1	5, B2	b-1	2095 (A, B)	1225.4	1076.101 (3)	1076.101	1	5	4	2	H, CoreF(1225.4)
					b-1 (2)	2146	1225.6	1613.652 (2)	1613.648	1	5	4	2	H, CoreF(1225.6)
					b-2	**2166 (A, B, C)**	**1224.5**	**1173.132 (3)**	**1173.133**	**1**	**5**	**4**	**3**	**H, CoreF(1224.5), diSia(582.7) [Figure 5, B1]**
						– (A)	1224.5	1759.195 (2)	1759.196	1	5	4	3	CoreF(1224.5), diSia(583.0)
					b-3	2235 (A)	1224.5	1270.166 (3)	1270.165	1	5	4	4	C, CoreF(1224.5), diSia(583.0)
						– (A)	1225.6	1367.199 (3)	1367.196	1	5	4	5	C, CoreF(1225.6), diSia(583.4)
	A	VAWLN[38]R (757.424)	11	5, A2		– (B)	961.5	987.930 (2)	987.930	0	5	2	0	Man-5
					a-1 (2)	3523 (A, B, C)	961.5	1068.956 (2)	1068.957	0	6	2	0	Man-6
					a-2 (2)	**3364 (A, B, C)**	**961.5**	**1149.986(2)**	**1149.983**	**0**	**7**	**2**	**0**	**Man-7 [Figure 5, A1]**
					a-3 (2)	3221 (A, B, C)	961.5	1231.010 (2)	1231.010	0	8	2	0	Man-8
					a-4 (2)	3413 (A, B, C)	961.5	1312.039 (2)	1312.036	0	9	2	0	Man-9
		DKNSKVAWLN[38]R (1329.715)	9	–	–	3074	1534.8	1011.774 (3)	1011.773	0	8	2	0	Man-8
		CVVEDKNSKVAWLN[38]R (1816.925)	15	–	–	4298	675.5(3)	1012.128 (3)	1012.123	0	5	2	0	Man-5
					–	4245	1011.2(2)	1120.160 (3)	1120.159	0	7	2	0	Man-7
					–	4208	1011.3(2)	1174.175 (3)	1174.176	0	8	2	0	Man-8
	C	ISN[108]ISSD (734.345)	–	–		– (A)	938.4	1296.508 (2)	1296.507	1	5	3	1	H, CoreF(1084.3) or $sL^{a/x}$ (454.2, 512.3, 657.2, 803.1)
						– (A)	938.5	1377.533 (2)	1377.534	1	6	3	1	H, CoreF(1084.2)
		ISN[108]ISSDVTVNE (1276.615)	14	5, C2	**c-1**	**3963**	**1480.6**	**1078.456 (3)**	**1078.454**	**2**	**4**	**5**	**0**	**C, CoreF(1627.4), bisectGN(1024.3) [Figure 5, C1]**
		GSN[120]VTLVCMANGRPEPVITWR (1603.745)	–	–	–	–	–	–	–	–	–	–	–	glycosylated [g]
	D	GQSSLTVTN[251]VTE (1234.604)	12	5, D2		– (A)	1438.6	1340.576 (2)	1340.576	1	3	4	0	CoreF(1584.6), bisectGN(1003.6)
						– (A)	1438.5	961.746 (3)	961.746	1	3	5	0	C, CoreF(1584.5), bisectGN(1004.1), BA-2
						– (A, B)	1438.5	1442.115 (2)	1442.116	1	3	5	0	C, CoreF(1584.5), bisectGN(1077.2), BA-2
					d-1	3630	1438.5	1002.088 (3)	1002.088	1	5	4	0	H, CoreF(1584.5) or $L^{a/x}$ (350.1, 512.1)
					d-2	**3646 (A, B, C)**	**1438.6**	**1064.451 (3)**	**1064.450**	**2**	**4**	**5**	**0**	**C, CoreF(1584.5), $L^{a/x}$ (350.3, 512.2) [Figure 5, D1]**
						– (C)	1439.6	1596.174 (2)	1596.171	2	4	5	0	C, CoreF(1585.6), 512(512.2)
						– (B)	1438.5	1167.154 (3)	1167.154	3	5	5	0	C, CoreF(1584.5), bisectGN(1004.1), $L^{b/y}$ (350.2, 512.1, 658.2)
					d-3	3742 (C)	1438.6	1215.502 (3)	1215.499	2	5	5	1	C, CoreF(1584.4), 512(512.3)
					d-4	3788 (C)	1438.6	1283.192 (3)	1283.193	2	5	6	1	C, CoreF(1584.5) ($sL^{a/x}$ (512.2, 657.2, 803.2))
					d-5	3668	1438.6	1385.898 (3)	1385.896	3	6	6	1	C, CoreF(1584.5) ($sL^{a/x}$ (512.2, 657.3, 803.1))
					d-6	3618 (A)	1438.5	1453.594 (3)	1453.589	3	6	7	1	C, CoreF(1584.6), 512(512.2)

Table 1: Continued

protein	peptides: sequence[a,b]	elution position	Figure	glycopeptides: peak no.[c]	scan in Figure 4A[d]	observed peptide-related ion[e]	observed *m/z* in SIM mode[b]	theoretical *m/z*[b]	*N*-glycan: deduced monosaccharide composition: dHex	Hex	HexNAc	NA	deduced structure[f] (diagnostic ion)
E	HYGN[259]YTCVAANK (1396.619)	4	5, E2	– (B)		801.8(2)	872.021 (3)	872.021	0	5	2	0	Man-5
				e-18 (2)	2884	1600.6	1307.532 (2)	1307.528	0	5	2	0	Man-5
				e-19 (2)	2949 (A)	1601.4	1421.587 (2)	1421.584	1	3	4	0	CoreF(1746.7), bisectGN(1085.6)
				e-1	2891 (A, C)	1600.6	1002.079 (3)	1002.076	1	4	4	0	H, CoreF(1746.6), bisectGN(1085.3)
				e-2	**2931 (A, B, C)**	**1600.6**	**1015.752 (3)**	**1015.752**	**1**	**3**	**5**	**0**	**C, CoreF(1746.6), bisectGN(1085.3), BA-2 [Figure 5, E1]**
				e-3	2859 (A)	1600.5	1037.089 (3)	1037.086	2	5	3	0	H, CoreF(1746.6), 512(512.1)
				e-4	2840	1600.6	1042.419 (3)	1042.418	1	6	3	0	H, 512(512.1)
				e-5	2878 (A)	1601.6	1050.764 (3)	1050.762	2	4	4	0	CoreF(1746.6), $L^{a/x}$ (350.2, 512.2), bisectGN(1085.5)
				e-6	2853 (A, B, C)	1600.5	1056.095 (3)	1056.094	1	5	4	0	H, CoreF(1747.7), bisectGN(1085.6)
				e-7	2994	1600.7	1085.433 (3)	1085.432	1	5	3	1	H, CoreF(1747.6) or 512(512.2)
				e-8	2821	1600.5	1091.107 (3)	1091.104	2	6	3	0	H, CoreF(1746.6), 512(512.2)
					– (A, C)	1601.6	1104.779 (3)	1104.780	2	5	4	0	H, CoreF(1747.8), bisectGN(1158.7), $L^{a/x}$ (349.9, 512.3)
				e-9	2847	1600.6	1110.111 (3)	1110.111	1	6	4	0	H, CoreF(1746.6) or $L^{a/x}$ (350.1, 512.3)
				e-10	2898 (A, C)	1601.7	1118.457 (3)	1118.455	2	4	5	0	C, CoreF(1746.7), bisectGN(1085.7), $L^{a/x}$ (350.2, 512.1)
				e-11	2989	1600.7	1139.452 (3)	1139.450	1	6	3	1	H, CoreF(1746.7)
				e-12	2808 (A)	1600.6	1153.467 (3)	1153.466	3	5	4	0	C, CoreF(1746.6), $L^{b/y}$ (658.2) or 512/512(512.1/512.3)
				e-13	2872	1600.4	1158.798 (3)	1158.797	2	6	4	0	H, CoreF(1747.7), $L^{a/x}$ (350.1, 512.1)
				e-14	3036	1601.7	1166.800 (3)	1166.801	1	4	5	1	C, CoreF(1747.4) or 512(512.1), bisectGN(1085.3)
				e-15	2983	1600.6	1201.813 (3)	1201.811	2	5	4	1	C, CoreF(1747.6), $sL^{a/x}$ (350.1, 512.2, 657.3, 803.2)
				e-16	2815	1600.6	1221.160 (3)	1221.159	3	5	5	0	C, CoreF(1747.6), bisectGN(1085.3), 512(512.2)
				e-17	3013	1600.7	1269.507 (3)	1269.505	2	5	5	1	C, CoreF(1746.7), bisectGN(1085.5), 512(512.1)

Table 1: Continued

protein	peptides: sequence[a,b]	elution position	Figure	glycopeptides: peak no.[c]	scan in Figure 4A[d]	observed peptide-related ion[e]	observed m/z in SIM mode[b]	theoretical m/z[b]	*N*-glycan: deduced monosaccharide composition: dHex	Hex	HexNAc	NA	deduced structure[f] (diagnostic ion)
F	LGVTN[272]ASLVLFR (1288.750)	24	5, F2		− (B)	1492.8	931.109 (3)	1396.160	0	3	5	0	C, bisectGN(1030.9)
				f-8 (2)	7644 (A, B)	1492.8	1396.161 (2)	1396.160	0	3	5	0	C, bisectGN(1031.0)
					− (B)	1492.8	979.795 (3)	979.795	1	3	5	0	C, CoreF(1638.9), bisectGN(1031.2), BA-2
				f-9 (2)	7577 (A, B, C)	1492.7	1469.189 (2)	1469.189	1	3	5	0	C, CoreF(1638.8), bisectGN(1031.2), BA-2
					− (A, B, C)	1492.9	1014.806 (3)	1014.806	2	4	4	0	C, CoreF(1640.0), 512(512.3)
				f-1	7558 (A, B, C)	1493.7	1033.813 (3)	1033.813	1	4	5	0	C, bisctGN(1031.1), CoreF(1639.8) or $L^{a/x}$ (350.2, 512.2)
					− (A)	1493.8	1550.215 (2)	1550.215	1	4	5	0	C, bisctGN(1031.6), CoreF(1640.0) or 512(512.2)
					− (A)	1492.9	1047.489 (3)	1047.488	1	3	6	0	C, CoreF(1638.8), bisectGN(1031.7)
					− (A, C)	1492.9	1063.151 (3)	1063.151	1	4	4	1	C, CoreF(1638.9)
					− (A)	1492.9	1082.157 (3)	1082.159	0	4	5	1	C, bisectGN(1031.0)
				f-2	**7468 (A, B, C)**	**1492.8**	**1082.499 (3)**	**1082.499**	**2**	**4**	**5**	**0**	**C, CoreF, bisectGN(1103.8) [Figure 5, F1]**
					− (A)	1492.8	1623.243 (2)	1623.244	2	4	5	0	C, CoreF(1638.9), bisectGN(1031.0), 512(513.2)
				f-3	7382 (A)	1492.8	1101.510 (3)	1101.506	1	4	6	0	C, bisectGN(1031.2), CoreF(1639.0) or $L^{a/x}$ (350.3, 512.2)
				f-4	7753 (A, B, C)	1492.7	1117.168 (3)	1117.169	1	5	4	1	C, CoreF(1638.8) or $sL^{a/x}$ (454.2, 512.3, 657.2, 803.1)
					− (A)	1493.9	1675.247 (2)	1675.250	1	5	4	1	H, CoreF(1638.9)
					− (A)	1493.8	1117.508 (3)	1117.509	3	5	4	0	C, CoreF(1639.4), $L^{b/y}$ (512.2, 658.5)
				f-5	7889 (A, C)	1492.8	1130.846 (3)	1130.845	1	4	5	1	C, CoreF(1638.7), bisectGN(1031.0, 1104.3)
					− (A)	1492.9	1136.517 (3)	1136.516	2	5	5	0	C, CoreF(1639.8), 512(512.2)
					− (A)	1494.0	1150.192 (3)	1150.192	2	4	6	0	C, CoreF(1639.1), $L^{a/x}$ (350.1, 512.2)
					− (A)	1493.1	1165.516 (3)	1165.515	0	5	4	2	C
				f-6	7815 (A, B, C)	1492.6	1165.856 (3)	1165.855	2	5	4	1	C, CoreF(1638.7), $sL^{a/x}$ (453.8, 512.1, 657.1, 803.2)
					− (A)	1493.3	1748.280 (2)	1748.279	2	5	4	1	C, CoreF(1639.9), 512(512.3)
				f-7	7765	1493.9	1184.864 (3)	1184.862	1	5	5	1	C, bisectGN(1032.0), CoreF(1639.3) or 512(512.2)
					− (A, C)	1492.7	1185.202 (3)	1185.202	3	5	5	0	C, CoreF(1639.1), $L^{b/y}$ (512.2, 658.4)
					− (A)	1492.7	1204.209 (3)	1204.209	2	5	6	0	C, CoreF(1638.9), $L^{a/x}$ (350.2, 512.2)
					− (A, C)	1493.2	1214.201 (3)	1214.201	1	5	4	2	C, CoreF(1639.8)

Table 1: Continued

protein	peptides		glycopeptides							*N*-glycan				
										deduced monosaccharide composition				
		sequence[a,b]	elution position	Figure	peak no.[c]	scan in Figure 4A[d]	observed peptide-related ion[e]	observed *m/z* in SIM mode[b]	theoretical *m/z*[b]	dHex	Hex	HexNAc	NA	deduced structure[f] (diagnostic ion)
						– (A)	1493.8	1233.548 (3)	1233.548	2	5	5	1	C, CoreF(1639.1), sL$^{a/x}$ (454.0, 512.6, 657.1, 803.0)
						– (A)	1493.8	1287.567 (3)	1287.566	2	6	5	1	C, CoreF(1639.4), 512(512.3)
						– (C)	1492.7	1336.251 (3)	1336.252	3	6	5	1	C, CoreF, 512(512.4)
						- (C)	1492.7	1384.602 (3)	1384.598	2	6	5	2	C, CoreF(1638.8) (sL$^{a/x}$ (454.9, 512.3, 657.1, 803.3))
		LGVTN^{272}ASLVLFRPGSVR (1785.026)	24	5, F2		– (C)	995.3(2)	1096.537 (3)	1096.534	0	3	5	0	C, bisectGN(1279.5)
					g-1	7508 (C)	995.4(2)	1145.223 (3)	1145.220	1	3	5	0	C, CoreF(1068.7), bisectGN(1352.3), BA-2
					g-2	7462 (C)	995.8(2)	1199.243 (3)	1199.238	1	4	5	0	C, CoreF(1069.2) or 512(512.2)
					g-3	7449 (C)	995.9(2)	1247.927 (3)	1247.924	2	4	5	0	C, CoreF(1068.4), bisectGN(1279.4), 512(512.2)
						– (C)	995.8(2)	1282.596 (3)	1282.594	1	5	4	1	C, 512(512.2)
						– (C)	995.4(2)	1331.283 (3)	1331.280	2	5	4	1	C, CoreF(1068.4), 512(512.3)
OBCAM	G	AMDN^{17}VTVR (904.444)	2	6, A2	h-1	2408 (A)	1254.5	1018.407 (3)	1018.405	1	5	3	2	H, CoreF(1254.5), (diSia(583.0))
						– (A, C)	1254.7	1086.098 (3)	1086.099	1	5	4	2	CoreF(1254.7)
						– (A)	1254.5	1628.644 (2)	1628.644	1	5	4	2	C, CoreF(1254.5)
						– (A, B)	1254.7	1115.437 (3)	1115.437	1	5	3	3	H, CoreF(1254.7), diSia(583.0)
						– (A)	1254.5	1672.651 (2)	1672.652	1	5	3	3	H, CoreF(1254.5), diSia(583.3)
						– (A)	1254.6	1169.454 (3)	1169.455	1	6	3	3	H, CoreF(1254.6), diSia(583.0)
					h-2	2473 (A, B, C)	1254.5	1183.131 (3)	1183.130	1	5	4	3	H, CoreF(1254.5) or 512(512.2), diSia(582.6)
					h-3	**2719 (C)**	**1254.5**	**1280.163 (3)**	**1280.162**	**1**	**5**	**4**	**4**	**C, CoreF(1254.5), diSia(582.9) [Figure 6, A1]**
						– (C)	1108.6	1377.198 (3)	1377.194	1	5	4	5	
	A	VAWLN^{43}R (757.424)	11	5, A2		– (B)	961.5	987.930 (2)	987.930	0	5	2	0	Man-5
					a-1 (2)	3523 (A, B, C)	961.5	1068.956 (2)	1068.957	0	6	2	0	Man-6
					a-2 (2)	**3364 (A, B, C)**	**961.5**	**1149.986(2)**	**1149.983**	**0**	**7**	**2**	**0**	**Man-7 [Figure 5, A1]**
					a-3 (2)	3221 (A, B, C)	961.5	1231.010 (2)	1231.010	0	8	2	0	Man-8
					a-4 (2)	3413 (A, B, C)	961.5	1312.039 (2)	1312.036	0	9	2	0	Man-9
		VHLIVQVPPQIMN^{113}ISSD (1889.008)	–	–	–	–	–	–	–	–	–	–	–	glycosylated [g]
		VHLIVQVPPQIMN^{113}ISSDITVNE (2445.294)	–	–	–	–	–	–	–	–	–	–	–	glycosylated [g]
	H	ISTLTFFN^{258}VSE (1256.629)	25	6, B2		– (A)	1460.6	1351.589 (2)	1351.589	1	3	4	0	CoreF(1606.3), bisectGN(1087.8)
						– (B)	1460.5	969.088 (3)	969.088	1	3	5	0	C, CoreF(1606.5), bisectGN(1088.6), BA-2
						– (A, C)	1461.5	1453.128 (2)	1453.128	1	3	5	0	C, CoreF(1606.5), bisectGN(1088.4), BA-2

Table 1: Continued

protein	peptides: sequence[a,b]	elution position	Figure	glycopeptides: peak no.[c]	scan in Figure 4A[d]	observed peptide-related ion[e]	observed m/z in SIM mode[b]	theoretical m/z[b]	*N*-glycan: deduced monosaccharide composition: dHex	Hex	HexNAc	NA	deduced structure[f] (diagnostic ion)
					− (A, B, C)	1461.7	1071.792 (3)	1071.792	2	4	5	0	C, (CoreF(1606.5), $L^{a/x}$ (350.1, 512.2)) or ($L^{b/y}$ (658.4))
					− (A, C)	1460.5	1607.183 (2)	1607.184	2	4	5	0	C, 512(512.3)
					− (C)	1460.5	1120.138 (3)	1120.137	1	4	5	1	C, CoreF(1606.5)
					− (A, C)	1460.5	1155.148 (3)	1155.148	2	5	4	1	C, CoreF(1606.6) ($sL^{a/x}$ (349.2, 512.2, 804.1)
					− (A, B)	1460.5	1174.494 (3)	1174.495	3	5	5	0	C, CoreF(1606.5), $L^{b/y}$ (350.7, 512.3, 658.2)
					− (A, C)	1461.4	1187.831 (3)	1187.831	1	4	6	1	C, CoreF(1606.6) or $sL^{a/x}$ (350.1, 512.5, 657.1, 803.1)
					− (C)	1460.5	1222.842 (3)	1222.841	2	5	5	1	C, CoreF(1606.5), $sL^{a/x}$ (454.0, 512.2, 803.2)
				i-1	**8712 (A, B, C)**	**1460.5**	**1290.538 (3)**	**1290.534**	**2**	**5**	**6**	**1**	**C, CoreF(1606.6) ($sL^{a/x}$ (454.2, 512.2, 657.1, 803.3) [Figure 6, B1]**
				i-2	8541 (A, C)	1460.5	1393.239 (3)	1393.238	3	6	6	1	C, CoreF(1606.5), 512(512.2)
1	YGN[266]YTCVATNK (1289.571)	7	6, C2		− (A)	1493.6	1254.003 (2)	1254.004	0	5	2	0	Man-5
					− (A)	1493.6	1368.060 (2)	1368.060	1	3	4	0	CoreF(1639.6), bisectGN(1031.5)
					− (B)	1493.6	980.068 (3)	980.069	1	3	5	0	C, CoreF(1639.6), bisectGN(1032.2), BA-2
				j-4 (2)	3156 (A, B, C)	1493.6	1469.602 (2)	1469.599	1	3	5	0	C, CoreF(1639.6), bisectGN(1105.0), BA-2
					− (C)	1493.6	1015.082 (3)	1015.079	2	4	4	0	CoreF(1639.5), $L^{a/x}$ (350.2, 512.1), bisectGN(1105.1)
				j-1	3048 (A)	1494.6	1082.774 (3)	1082.772	2	4	5	0	C, CoreF(1640.5), $L^{a/x}$ (350.4, 512.2), bisectGN(1105.9) [Figure 6, C1]
				j-2	3030	1493.6	1117.783 (3)	1117.783	3	5	4	0	H, CoreF(1639.5), $L^{b/y}$ (350.3, 512.1, 658.1)
				j-3	3024	1494.6	1185.478 (3)	1185.476	3	5	5	0	C, CoreF(1639.6), $L^{a/x}$ (349.0, 512.1), bisectGN(1032.7)
	DYGN[266]YTCVATNK (1404.598)	13	−		− (A)	1608.6	1311.517 (2)	1311.518	0	5	2	0	Man-5
					3885 (A)	1609.7	1018.412 (3)	1018.411	1	3	5	0	C, CoreF(1754.5), bisectGN(1089.6), BA-2
					− (A)	1608.6	1527.113 (2)	1527.113	1	3	5	0	C, CoreF(1754.6), bisectGN(1089.1), BA-2
					− (A)	1608.6	1121.115 (3)	1121.115	2	4	5	0	C, CoreF(1754.7), $L^{a/x}$ (350.3, 512.3)
					− (A)	1608.7	1156.125 (3)	1156.125	3	5	4	0	H, CoreF(1754.8), 512(512.2)
	KDYGN[266]YTCVATNK (1532.693)	6	−		− (C)	1736.7	1489.625 (2)	1489.621	1	3	4	0	CoreF(1882.8), bisectGN(1225.1)
					3510 (C)	1737.8	1061.109 (3)	1061.109	1	3	5	0	C, CoreF(1884.9), bisectGN(1226.7), BA-2
					3133	1737.7	1150.141 (3)	1150.137	2	5	4	0	H, CoreF(1883.8), $L^{a/x}$ (350.4, 512.2)

Table 1: Continued

protein	peptides		glycopeptides							*N*-glycan				
										deduced monosaccharide composition				
		sequence[a,b]	elution position	Figure	peak no.[c]	scan in Figure 4A[d]	observed peptide-related ion[e]	observed *m/z* in SIM mode[b]	theoretical *m/z*[b]	dHex	Hex	HexNAc	NA	deduced structure[f] (diagnostic ion)
						− (C)	1736.5	1163.814 (3)	1163.813	2	4	5	0	C, CoreF(1882.7), bisectGN(1153.7), $L^{a/x}$ (350.3, 512.2)
						3054	1737.6	1198.826 (3)	1198.823	3	5	4	0	C, CoreF(1884.7), $L^{a/x}$ (350.1, 512.2)
						3458	1737.1	1212.160 (3)	1212.159	1	4	5	1	C, CoreF(1883.9), bisectGN(1226.3)
						3295	1737.0	1247.170 (3)	1247.169	2	5	4	1	CoreF(1882.8), $sL^{a/x}$ (453.8, 512.2, 657.2, 803.2)
	J	LGNTN[279]ASITLYGPGAVID (1774.910)	−	−		− (A)	1978.7	1093.161 (3)	1093.162	0	3	5	0	C
						− (A)	1979.8	1141.848 (3)	1141.848	1	3	5	0	C, CoreF(1062.9), bisectGN(1273.8), BA-2
neurotrimin	G	AMDN[12]VTVR (904.444)	2	6, A2	h-1	2408 (A)	1254.5	1018.407 (3)	1018.405	1	5	3	2	H, CoreF(1254.5), (diSia(583.0))
						− (A, C)	1254.7	1086.098 (3)	1086.099	1	5	4	2	CoreF(1254.7)
						− (A)	1254.5	1628.644 (2)	1628.644	1	5	4	2	C, CoreF(1254.5)
						− (A, B)	1254.7	1115.437 (3)	1115.437	1	5	3	3	H, CoreF(1254.7), diSia(583.0)
						− (A)	1254.5	1672.651 (2)	1672.652	1	5	3	3	H, CoreF(1254.5), diSia(583.3)
						− (A)	1254.6	1169.454 (3)	1169.455	1	6	3	3	H, CoreF(1254.6), diSia(583.0)
					h-2	2473 (A, B, C)	1254.5	1183.131 (3)	1183.130	1	5	4	3	H, CoreF(1254.5) or 512(512.2), diSia(582.6)
					h-3	**2719 (C)**	**1254.5**	**1280.163 (3)**	**1280.162**	**1**	**5**	**4**	**4**	**C, CoreF(1254.5), diSia(582.9) [Figure 6, A1]**
						− (C)	1108.6	1377.198 (3)	1377.194	1	5	4	5	
	A	VAWLN[38]R (757.424)	11	5, A2	*	− (B)	961.5	987.930 (2)	987.930	0	5	2	0	Man-5
					a-1 (2)	3523 (A, B, C)	961.5	1068.956 (2)	1068.957	0	6	2	0	Man-6
					a-2 (2)	**3364 (A, B, C)**	**961.5**	**1149.986(2)**	**1149.983**	**0**	**7**	**2**	**0**	**Man-7 [Figure 5, A1]**
					a-3 (2)	3221 (A, B, C)	961.5	1231.010 (2)	1231.010	0	8	2	0	Man-8
					a-4 (2)	3413 (A, B, C)	961.5	1312.039 (2)	1312.036	0	9	2	0	Man-9
		GNN[120]ISLTCIATGR (1375.688)	−	−	−	−	−	−	−	−	−	−	−	glycosylated [g]
		GNN[120]ISLTCIATGRPE (1601.783)	−	−	−	−	−	−	−	−	−	−	−	glycosylated [g]
		GNN[120]ISLTCIATGRPEPTVTWR (2285.159)	−	−	−	−	−	−	−	−	−	−	−	glycosylated [g]
	K	LTFFN[252]VSE (955.465)	20	7, A2	k-4 (2)	6885 (A)	1159.4	1086.954 (2)	1086.951	0	5	2	0	Man-5
						− (A)	1159.4	1180.493 (2)	1180.494	1	4	3	0	CoreF(1305.5)
					k-6 (2)	6824 (A, B)	1159.4	1201.011 (2)	1201.007	1	3	4	0	CoreF(1305.4)
						− (A)	1159.5	1261.520 (2)	1261.520	1	5	3	0	H, CoreF(1305.3)
					k-7 (2)	6819 (A, B)	1159.4	1302.551 (2)	1302.546	1	3	5	0	C, CoreF(1305.3), bisectGN(864.6), BA-2
						− (A)	1159.5	1334.551 (2)	1334.549	2	5	3	0	H, CoreF(1305.3), 512(512.3)
						− (A, B)	1159.4	1355.062 (2)	1355.062	2	4	4	0	CoreF(1305.2), 512(512.4)
						− (A, B)	1159.5	1363.059 (2)	1363.060	1	5	4	0	H, bisectGN(864.4), CoreF(1305.4) or 512(511.9)
						− (A)	1160.4	1407.068 (2)	1407.068	1	5	3	1	H, CoreF(1306.4)
						− (A)	1159.8	1415.576 (2)	1415.575	2	6	3	0	H, CoreF(1305.3)

Table 1: Continued

protein	peptides: sequence[a,b]	elution position	Figure	glycopeptides: peak no.[c]	scan in Figure 4A[d]	observed peptide-related ion[e]	observed m/z in SIM mode[b]	theoretical m/z[b]	*N*-glycan: deduced monosaccharide composition: dHex	Hex	HexNAc	NA	deduced structure[f] (diagnostic ion)
					– (B)	1159.4	957.728 (3)	957.728	2	5	4	0	H, CoreF(1305.7), $L^{a/x}$ (350.3, 512.1)
				k-8 (2)	6735 (A, B)	1159.3	1436.093 (2)	1436.089	2	5	4	0	H, CoreF(1305.4), 512(512.3)
					– (A)	1159.7	1444.089 (2)	1444.086	1	6	4	0	H, CoreF(1305.4)
					– (B)	1159.5	971.404 (3)	971.404	2	4	5	0	C, CoreF(1305.4), 512(512.3)
				k-9 (2)	6725 (A, B)	1159.5	1456.605 (2)	1456.602	2	4	5	0	C, (CoreF(1305.4), 512(512.1)) or $L^{b/y}$ (658.2), bisetGN(864.3)
					– (A)	1160.6	1480.098 (2)	1480.097	2	5	3	1	H, CoreF(1305.3), $sL^{a/x}$ (454.3, 512.2, 657.1, 803.2)
				k-1	6590	1159.3	1006.417 (3)	1006.414	3	5	4	0	C, CoreF(1305.2), $L^{b/y}$ (658.3)
				k-2	**6658**	**1159.4**	**1011.747 (3)**	**1011.746**	**2**	**6**	**4**	**0**	**H, CoreF(1305.3), $L^{a/x}$ (350.3, 512.1), bisectGN(865.4) [Figure 7, A1]**
					– (A)	1159.3	1517.117 (2)	1517.115	2	6	4	0	H, CoreF(1305.3), 512(512.1)
					– (A, B)	1160.4	1019.749 (3)	1019.749	1	4	5	1	C, CoreF(1305.4)
					– (A)	1159.5	1054.760 (3)	1054.760	2	5	4	1	H, CoreF(1305.5), 512(512.2)
				k-3	6533	1159.5	1074.108 (3)	1074.107	3	5	5	0	C, CoreF(1305.4), $L^{b/y}$ (658.1)
					– (A)	1159.4	1087.442 (3)	1087.443	1	4	6	1	C, CoreF(1305.4)
					– (A)	1159.5	1122.453 (3)	1122.453	2	5	5	1	C, CoreF(1305.5), 512(512.2)
				k-5	6782 (A, B)	1159.4	1190.151 (3)	1190.146	2	5	6	1	C, CoreF(1305.3), $sL^{a/x}$ (350.2, 512.2, 657.1, 803.2)
L	YGN[260]YTCVASNK (1275.555)	5	7, B2	**l-1**	**2954 (A, B, C)**	**1480.6**	**1078.100 (3)**	**1078.100**	**2**	**4**	**5**	**0**	**C, CoreF(1626.6), bisectGN(1024.9), $L^{a/x}$ (350.3, 512.1) [Figure 7, B1]**
				l-1 (2)	2960 (A)	1479.5	1616.649 (2)	1616.647	2	4	5	0	C, CoreF(1626.6), bisectGN(1024.4), 512(512.2)
				l-2	2918 (A)	1479.6	1113.114 (3)	1113.111	3	5	4	0	H, CoreF(1625.5), $L^{b/y}$ (658.1)
					– (A)	1480.6	1126.446 (3)	1126.446	1	4	5	1	C, CoreF(1626.6)
				l-3	3093	1478.0	1161.457 (3)	1161.457	2	5	4	1	H, CoreF(1626.7), $sL^{a/x}$ (350.4, 512.1, 657.2, 803.1)
				l-4	2905 (A, B)	1479.6	1180.806 (3)	1180.804	3	5	5	0	C, CoreF(1625.6), bisectGN(1024.6), $L^{a/x}$ (350.0, 512.3)
	HDYGN[260]YTCVASNK (1527.641)	8	–		3254 (A, C)	1732.4	1059.426 (3)	1059.425	1	3	5	0	C, CoreF(1878.7), bisectGN(1150.6), BA-2
					3176 (A, C)	1731.6	1162.128 (3)	1162.129	2	4	5	0	C, (CoreF(1878.7), $L^{a/x}$ (350.1, 512.2)) or $L^{b/y}$ (658.4), bisectGN(1223.8)

Table 1: Continued

protein	peptides		glycopeptides							*N*-glycan				
										deduced monosaccharide composition				
		sequence[a,b]	elution position	Figure	peak no.[c]	scan in Figure 4A[d]	observed peptide-related ion[e]	observed *m/z* in SIM mode[b]	theoretical *m/z*[b]	dHex	Hex	HexNAc	NA	deduced structure[f] (diagnostic ion)
						– (C)	1732.7	1197.144 (3)	1197.139	3	5	4	0	H, CoreF(1877.7), $L^{b/y}$ (512.2, 658.2), bisectiGN(1149.1)
						3439	1731.7	1210.475 (3)	1210.475	1	4	5	1	C, CoreF(1877.8), bisectGN(1222.6)
						3383	1732.8	1245.488 (3)	1245.485	2	5	4	1	H, CoreF(1879.7), $sL^{a/x}$ (453.9, 512.2, 657.2, 803.3)
						3080 (C)	1732.7	1264.834 (3)	1264.833	3	5	5	0	C, CoreF(1878.7), bisectGN(1223.4), 512(512.1)
						3553	1731.9	1293.835 (3)	1293.831	1	5	4	2	H, CoreF(1877.6), bisectGN(1150.5)
						3560	1731.9	1294.175 (3)	1294.171	3	5	4	1	C, CoreF(1877.7)
	M	LGHTN[273]ASIMLFGPGAVSE (1799.888)	23	7, C2	**m-1**	**7299 (C)**	**1002.6(2)**	**1101.491 (3)**	**1101.488**	**0**	**3**	**5**	**0**	**C, bisectGN(1286.7) [Figure 7, C1]**
						– (C)	1003.1(2)	1141.835 (3)	1141.830	0	5	4	0	H, bisectGN(1286.5)
					m-2	7227 (C)	1002.6(2)	1150.176 (3)	1150.174	1	3	5	0	C, CoreF(1075.6), bisectGN(1357.6), BA-2
					m-3	7210	1002.7(2)	1190.520 (3)	1190.516	1	5	4	0	H, CoreF(1075.4) or 512(512.0), bisectGN(1359.1)
					m-4	7186	1002.8(2)	1244.537 (3)	1244.534	1	6	4	0	H, 512(512.2)
Kilon	N	GAWLN[36]R (715.377)	3	8, A2		– (B)	919.5	966.907 (2)	966.907	0	5	2	0	Man-5
					n-1 (2)	**2664 (A, B, C)**	**919.5**	**1047.934 (2)**	**1047.933**	**0**	**6**	**2**	**0**	**Man-6 [Figure 8, A1]**
					n-2 (2)	2706 (A, B, C)	919.5	1128.960 (2)	1128.960	0	7	2	0	Man-7
					n-3 (2)	2679 (A, B, C)	919.4	1209.988 (2)	1209.986	0	8	2	0	Man-8
		CYLEDGASGAWLN[36]R (1738.810)	18	–		5234	972.3	1040.101 (3)	1040.102	0	6	2	0	Man-6
	O	GTN[118]VTLTCLATGKPE (1560.782)	16	8, B2	**o-1**	**4760**	**1765.8**	**1070.475 (3)**	**1070.472**	**1**	**3**	**5**	**0**	**C, CoreF(1910.8), bisectGN(1167.3), BA-2 [Figure 8, B1]**
					o-2	4683	1764.7	1105.485 (3)	1105.483	2	4	4	0	CoreF(1910.9), bisectGN(1167.8), 512(512.2)
					o-3	4710 (C)	1765.7	1173.176 (3)	1173.176	2	4	5	0	C, CoreF(1911.9), bisectGN(1167.3), 512(512.1)
					o-4	4638	1765.8	1275.880 (3)	1275.879	3	5	5	0	C, CoreF(1910.9), 512(512.1)
					o-5	4857 (C)	1765.0	1324.227 (3)	1324.225	2	5	5	1	C, CoreF(1910.8), 512(512.1)
						– (C)	1764.9	1401.911 (3)	1401.910	1	5	4	3	C, CoreF(1911.0)
	P	LFNGQQGIIIQN[238]FSTR (1834.969)	22	8, C2	**p-1**	**7203 (C)**	**1020.3(2)**	**1018.138 (3)**	**1018.138**	**0**	**5**	**2**	**0**	**Man-5 [Figure 8, C1]**
		RLFNGQQGIIIQN[238]FSTR (1991.070)	21	–		6895 (C)	1098.3(2)	1070.171 (3)	1070.172	0	5	2	0	Man-5
		KRLFNGQQGIIIQN[238]FSTR (2119.165)	19	–		6165 (C)	1162.4(2)	1112.871 (3)	1112.870	0	5	2	0	Man-5
	Q	SILTVTN[249]VTQE (1203.635)	17	8, D2	q-8 (2)	5086 (A, C)	1407.5	1211.037 (2)	1211.036	0	5	2	0	Man-5
						– (B)	1407.7	883.729 (3)	883.730	1	3	4	0	CoreF(1553.5), bisectGN(1061.5)

Table 1: Continued

peptides		glycopeptides							*N*-glycan				
									deduced monosaccharide composition				
protein	sequence[a,b]	elution position	Figure	peak no.[c]	scan in Figure 4A[d]	observed peptide-related ion[e]	observed *m/z* in SIM mode[b]	theoretical *m/z*[b]	dHex	Hex	HexNAc	NA	deduced structure[f] (diagnostic ion)
				q-10 (2)	5059 (A, C)	1407.4	1325.094 (2)	1325.092	1	3	4	0	CoreF(1553.5) or 512(512.2), bisectGN(988.6)
					– (B)	1407.6	951.423 (3)	951.423	1	3	5	0	C, CoreF(1553.6), bisectGN(988.6), BA-2
					– (A)	1407.6	1426.632 (2)	1426.631	1	3	5	0	C, CoreF(1553.5), bisectGN(988.2), BA-2
				q-11 (2)	4950 (A, C)	1407.5	1458.635 (2)	1458.634	2	5	3	0	H, CoreF(1553.4), 512(512.2)
					– (B)	1407.3	991.765 (3)	991.765	1	5	4	0	H, CoreF(1553.6)
					– (A)	1407.6	1487.143 (2)	1487.144	1	5	4	0	H, CoreF(1553.4)
				q-1	5126 (A)	1407.5	1021.106 (3)	1021.104	1	5	3	1	H, CoreF(1553.4) or 512(512.2)
					– (A)	1407.6	1531.153 (2)	1531.152	1	5	3	1	H, CoreF(1553.6) or 512(512.0)
				q-2	4885 (C)	1407.4	1026.777 (3)	1026.776	2	6	3	0	H, CoreF(1553.5), $L^{6'}$ (350.3, 512.2)
				q-2 (2)	4919 (C)	1407.6	1539.663 (2)	1539.660	2	6	3	0	H, CoreF(1554.2), 512(512.1)
				q-3	5010 (A, C)	1407.5	1040.453 (3)	1040.451	2	5	4	0	H, CoreF(1553.6), $L^{6'}$ (350.2, 512.1)
					– (A)	1407.5	1560.174 (2)	1560.173	2	5	4	0	H, CoreF(1553.4), 512(512.2)
				q-4	**4944 (A, C)**	**1406.6**	**1054.128 (3)**	**1054.127**	**2**	**4**	**5**	**0**	**C, CoreF(1552.6)s, $L^{6'}$ (350.2, 512.1) [Figure 8, D1]**
					– (A)	1407.6	1580.687 (2)	1580.687	2	4	5	0	C, CoreF(1553.6), 512(512.2)
					– (A)	1407.5	1075.121(3)	1075.122	1	6	3	1	H, CoreF(1554.6)
					– (A)	1407.6	1612.180 (2)	1612.179	1	6	3	1	H, CoreF(1554.5)
				q-5	4827	1407.5	1089.139 (3)	1089.137	3	5	4	0	H, CoreF(1553.6), 512(512.1)
					– (A)	1407.5	1094.469 (3)	1094.469	2	6	4	0	H, CoreF(1554.3), $L^{6'}$ (350.3, 512.2)
					– (A)	1407.3	1102.473 (3)	1102.473	1	4	5	1	C, CoreF(1552.7)
				q-6	5032	1407.5	1137.486 (3)	1137.483	2	5	4	1	C, CoreF(1553.3), 512(512.2)
				q-7	4869 (A)	1407.6	1156.832 (3)	1156.830	3	5	5	0	C, CoreF(1553.5)
					– (A)	1407.6	1170.166 (3)	1170.166	1	4	6	1	C, CoreF(1553.3) or ($sL^{6'}$ (512.4, 803.6)
				q-9	5054 (A)	1407.4	1272.870 (3)	1272.869	2	5	6	1	C, CoreF(1553.5) ($sL^{6'}$ (454.1, 512.2, 657.2, 803.2))
R	HFGN[257]YTCVAANK (1380.624)	10	8, E2		– (B)	793.2(2)	866.690 (3)	866.690	0	5	2	0	Man-5
				r-7 (2)	3214 (C)	1584.7	1299.536 (2)	1299.531	0	5	2	0	Man-5
				r-1	3339 (C)	1584.6	1010.422 (3)	1010.420	1	3	5	0	C, CoreF(1730.6), bisectGN(1077.0), BA-2
				r-2	**3162 (A, C)**	**1584.7**	**1050.764 (3)**	**1050.762**	**1**	**5**	**4**	**0**	**H, CoreF(1730.5), bisectGN(1077.7) [Figure 8, E1]**
				r-3	3139 (A, C)	1585.9	1085.774 (3)	1085.772	2	6	3	0	H, CoreF(1730.8), $L^{6'}$ (350.2, 512.2)

Table 1: Continued

protein	peptides		glycopeptides					*N*-glycan				
	sequence[a,b]	elution position	Figure	peak no.[c]	scan in Figure 4A[d]	observed peptide-related ion[e]	observed *m/z* in SIM mode[b]	theoretical *m/z*[b]	deduced monosaccharide composition				deduced structure[f] (diagnostic ion)
									dHex	Hex	HexNAc	NA	
				r-4	3208 (C)	1585.7	1099.450 (3)	1099.448	2	5	4	0	H, CoreF(1731.7), $L^{a/x}$ (350.1, 512.1)
				r-5	3189	1584.7	1104.784 (3)	1104.780	1	6	4	0	H, CoreF(1730.6) or $L^{a/x}$ (350.4, 512.0)
				r-6	3144 (A)	1585.6	1113.127 (3)	1113.123	2	4	5	0	C, CoreF(1730.8), $L^{a/x}$ (350.1, 512.2)
					– (A)	1585.8	1134.118 (3)	1134.118	1	6	3	1	H, CoreF(1730.6) or 512(512.3)
					– (A)	1584.5	1153.466 (3)	1153.466	2	6	4	0	H, CoreF(1731.6), $L^{a/x}$ (350.1, 512.2)

[a] Theoretical peptide mass indicated in parentheses. [b] Monoisotopic values. [c] Peaks are numbered in decreasing order of their calculated mass. All glycopeptides are triply charged except for doubly charged ions indicated by (2) after the peak number. [d] Glycopeptides were characterized on the basis of alternative LC−MS^n runs with conditions indicated in parentheses (A, a C30 column, scan range of *m/z* 1000−2000; B, a C30 column, scan range of *m/z* 700−2000; C, a C18 column, scan range of *m/z* 1000−2000). [e] Y_i^{n+} or $Y_{i\alpha/\beta}^{n+}$, [(peptide + HexNAc + *n*H)/*n*]$^{n+}$; or $Y_{i\alpha}^{n+}$, [(peptide + HexNAc + dHex + *n*H)/*n*]$^{n+}$. All peptide-related ions are singly charged except for doubly or triply charged ions indicated by (2) or (3). [f] Structures are deduced by MS^n: C, complex-type oligosaccharide; H, hybrid-type oligosaccharide; Man-5-9, high mannose-type oligosaccharide containing 5−9 mannose residues; CoreF, trimannosylcore fucose; bisectGN, bisecting GlcNAc; diSia, disialic acid; $L^{a/x}$, Lewis a/x structure; $sL^{a/x}$, sialylated Lewis a/x structure; $L^{b/y}$, Lewis b/y structure; 512, glycan motif consisting of $dHex_1Hex_1HexNAc_1$. The structure in parentheses indicates the possible structures to be contained in the glycopeptide. [g] Glycosylation was confirmed by Asn−Asp conversion upon PNGase F digestion.

integrated mass spectrum (peaks f-1−9 and g-1−3 in panel F2 of Figure 5) and their MS/MS spectra suggested that complex-type oligosaccharides including $Le^{a/x}$ or $Le^{b/y}$ -modified and/or bisected oligosaccharides and BA-2 are attached to Asn272 (Table 1F).

(vii) Asn287. The MS/MS spectra of GPI-linked peptides were selected from all MS data on the basis of the GPI-characteristic oxonium ions, such as GlcN-Ino-PO_4^+ (*m/z* 422). The structures of the GPI moieties were characterized from their product ions appearing in the MS/MS spectra, and their peptide portions were identified by comparing their observed masses with the theoretical masses of predicted peptides. Figure 4B shows the TIC obtained by GCC-LC−MS^n for the hydrophilic glycopeptides. On the basis of the presence of GPI-characteristic oxonium ions, the MS data of GPI-linked peptides were located at position 26. The 9.5% of spectra generated at elution position 26 were assigned to those of GPI-linked peptides of LAMP, OBCAM, and neurotrimin.

Figure 5G shows one of the MS/MS spectra acquired at position 26 (precursor ion, $[M + 2H]^{2+}$ at *m/z* 902.5; peak L2 in Figure 4C). On the basis of the GPI-characteristic oxonium ions, such as NH_2Et-PO_4-Man-$GlcN^+$ (*m/z* 447.2), NH_2Et-PO_4-(HexNAc-)Man-$GlcN^+$ (*m/z* 650.3), NH_2Et-PO_4-(HexNAc-)Man-GlcN-Ino-PO_4^+ (*m/z* 910.2), NH_2Et-PO_4-(HexNAc-)(Hex-)Man-GlcN-Ino-PO_4^+ (*m/z* 1072.2), and GlcN-Ino-PO_4^+ (*m/z* 422.2), this peptide was identified as the GPI-linked peptide. The product ion at *m/z* 328.3 was assigned to GlN^{287}-NH-Et^+ on the basis of the fragments that arose by successive cleavages of HexNAc (*m/z* 1600.4), Ino-PO_4 (*m/z* 1340.5), GlcN (*m/z* 1178.3), Man-PO_4-$EtNH_2$ and Hex (*m/z* 732.2), Hex (*m/z* 570.2), and PO_4-Hex (*m/z* 328.3). In addition, the product ions at *m/z* 732.3 and 1072.2 suggested the existence of HexNAc-(NH_2Et-PO_4-)(Hex)-Man3 in the core structure of GPI (inset of Figure 5G). The presence of a positional isomer was inferred from the acquisition of two different MS/MS spectra of GPI-linked peptides (precursor ion $[M + 2H]^{2+}$, *m/z* 903) at different elution times (Table 2). The alternative runs also suggested the presence of a Hex-Man1 and HexNAc-(Hex-)(NH_2Et-PO_4-)Man3 (peak L1, data not shown, Table 2), and a nonsubstituted Man1 and HexNAc-(NH_2Et-PO_4-)Man3 (data not shown, Table 2) in the GPI core structure.

Glycosylation Analysis of OBCAM. OBCAM has six potential N-glycosylation sites at Asn17, -43, -113, -258, -266, and -279, and the predicted linkage site of GPI is Asn295. From the peptide-related ions, peptides eluted at positions 2, 25, and 7 were estimated to be glycopeptides containing Asn17, -258, and -266, respectively (panels A1−C1 of Figure 6). Panels A2−C2 of Figure 6 show the integrated mass spectrum of glycopeptides obtained from positions 2, 25, and 7, respectively. The glycopeptide containing Asn43 is identical to $VAWLN^{38}R$ in LAMP. From the glycosylation at Asn38 in LAMP, Man-5-9 were inferred to be attached to Asn43 (panel A2 of Figure 5 and Table 1A). Although the MS/MS spectrum of the glycopeptide containing Asn113 (VHLIVQVPPQIMN[113]ISSD) was not acquired, glycosylation at Asn113 was corroborated by detection of VHLIVQVPPQIMD^{113}ISSD after PNGase F treatment (data not shown). The feature of glycosylation at Asn279 was elucidated on the basis of the MS/MS spectra of glycosylated LGNTN^{279}ASITLYGPGAVID which was

Table 2: Summary of GPI Structure in LAMP, OBCAM, and Neurotrimin

protein	peptide (theoretical MW[b])	peak no. in Figure 4C	scan in Figure 4B	GPI-linked peptide: observed peptide-related ion[b] (charge state)	GPI-linked peptide: observed *m/z*[b] (charge state)	GPI-linked peptide: calculated mass	GPI moiety: calculated mass	GPI moiety: deduced glycan composition: core	Man1	Man3				
									Hex	Hex	HexNAc	P-EtNH$_2$	theoretical MW[b]
LAMP	GIN[287] (302.3)	L1	3863	328.3 (1)	983.6 (2)	1965.1	1680.9	1	1	1	1	1	1681.3
		L2	**3828[c] (Figure5G)**	328.3 (1)	**902.5 (2)**	**1803.0**	**1518.8**	**1**	**0**	**1**	**1**	**1**	**1519.2**
			4040[c]	328.3 (1)	903.1 (2)	1804.2	1520.0	1	0	1	1	1	1519.2
			a	328.2 (1)	821.6 (2)	1641.1	1356.9	1	0	0	1	1	1357.0
OBCAM	GVN[295] (288.3)	**O1**	**3701 (Figure6D)**	314.3 (1)	**976.5 (2)**	**1951.0**	**1680.7**	**1**	**1**	1	**1**	**1**	**1681.3**
		O2	3633[d]	314.3 (1)	895.4 (2)	1788.7	1518.4	1	0	1	1	1	1519.2
			3853[d]	314.3 (1)	895.5 (2)	1788.9	1518.6	1	0	1	1	1	1519.2
		O3	3805	314.3 (1)	814.6 (2)	1627.1	1356.8	1	0	0	1	1	1357.0
neurotrimin	VNN[289] (345.4)	N1	3750	371.2 (1)	1004.8 (2)	2007.7	1680.3	1	1	1	1	1	1681.3
		N2	3741[e]	371.4 (1)	924.0 (2)	1846.1	1518.7	1	0	1	1	1	1519.2
			3896[e]	371.2 (1)	924.1 (2)	1846.1	1518.8	1	0	1	1	1	1519.2
		N3	**3873 (Figure7D)**	371.3 (1)	**842.8 (2)**	**1683.5**	**1356.1**	**1**	**0**	**0**	**1**	**1**	**1357.0**

[a] The structure of GPI was deduced by another LC−MS[n] run. [b] Average value. [c] Isomers. [d] Isomers. [e] Isomers.

acquired in an alternative run with the C30 column (scan range of *m/z* 1000−2000) (Table 1J).

(i) Asn 17. As shown in panel A1 of Figure 6, the glycopeptide that eluted at position 2 was assigned to AMDN[17]VTVR (and/or AMDN[12]VTVR in neurotrimin) glycosylated with dHex$_1$Hex$_5$HexNAc$_4$NeuAc$_4$ based on the $Y_{1\alpha}$ ion and the monoisotopic mass of the molecular ion. The attachment of three NeuAc residues in one branch of a biantennary complex type was suggested by the existence of characteristic B ions (*m/z* 495.2, 744.9, and 1239.2) (panel A1 of Figure 6). The molecular ions appearing in the integrated mass spectrum and their MS/MS spectra suggested that most of the glycans at Asn17 were disialic acid-conjugated oligosaccharides (peaks h-1−3 in panel A2 of Figure 6 and Table 1G).

(ii) Asn258. Panel B1 of Figure 6 shows the representative MS/MS spectrum of glycosylated ISTLTFFN[258]VSE that eluted at position 25. The monosaccharide composition (dHex$_2$Hex$_5$HexNAc$_6$NeuAc$_1$) implied two possible structures: a sLe$^{a/x}$ -modified core-fucosylated complex type and a Le$^{a/x}$ or antigen H-modified core-fucosylated and sialylated complex type (inset of panel B1 of Figure 6). The molecular ions (peaks i-1−2) in the integrated mass spectrum (panel B2 of Figure 6) and the detection of nonglycosylated ISTLTFFN[258]VSE revealed that Asn258 is partly glycosylated with the sLe$^{a/x}$ or Le$^{b/y}$-modified core-fucosylated complex type, and BA-2 (Table 1H).

(iii) Asn266. Panel C1 of Figure 6 shows the product ion spectra of the glycopeptide at position 7, the peptide portion of which was assigned to YGN[266]YTCVATNK on the basis of the $Y_{1\alpha/1\beta}$ ion in the MS/MS/MS spectrum. The glycan was characterized as the bisected and core-fucosylated complex-type oligosaccharide containing Le$^{a/x}$ structure from the monosaccharide composition (dHex$_2$Hex$_4$HexNAc$_5$), and the Le$^{a/x}$-, bisecting-, and core-fucose-related ions. The MS/MS spectra acquired with other glycoforms (peaks j-1−4 in panel C2 of Figure 6) together with the MS/MS spectra of the glycopeptides DYGN[266]YTCVATNK (position 13) and KDYGN[266]YTCVATNK (position 6) suggested that the Le$^{a/x}$-modified and/or bisected complex type and Man-5 were predominantly attached to Asn266 (Table 1I).

(iv) Asn295. On the basis of the GPI-characteristic oxonium ions and the peptide-related ion (*m/z* 314.3), the MS/MS spectrum of GPI-linked GVN[295] was picked out from position 26 (Figure 6D; precursor ion, *m/z* 976.5; peak O1 in Figure 4C). The fragments arising from the GPI moiety suggested the linkage of Hex to Man1, and HexNAc, Hex, and NH_2Et-PO_4 to Man3 in the core structure (Figure 6D, inset). Furthermore, the MS/MS spectrum of other GPI-linked GVN[295] (precursor ion, *m/z* 895; peak O2), which was picked out from position 26 based on the peptide-related ion, suggested that this GPI moiety contained HexNAc-(Hex)-(NH_2Et-PO_4-)Man3. Another MS/MS spectrum (precursor ion, *m/z* 814; peak O3) suggested the linkage of GPI moieties containing HexNAc-(NH_2Et-PO_4-)Man3 (Table 2). The existence of two isomers was suggested in peak O2 by the acquisition of two MS/MS spectra of GPI-GVN[295] (*m/z* 895) at different elution times.

Glycosylation Analysis of Neurotrimin. Neurotrimin contains seven potential N-glycosylation sites at Asn12, -38, -120, -184, -252, -260, and -273, and the predicted linkage site of GPI is Asn289. As the amino acid sequence in the

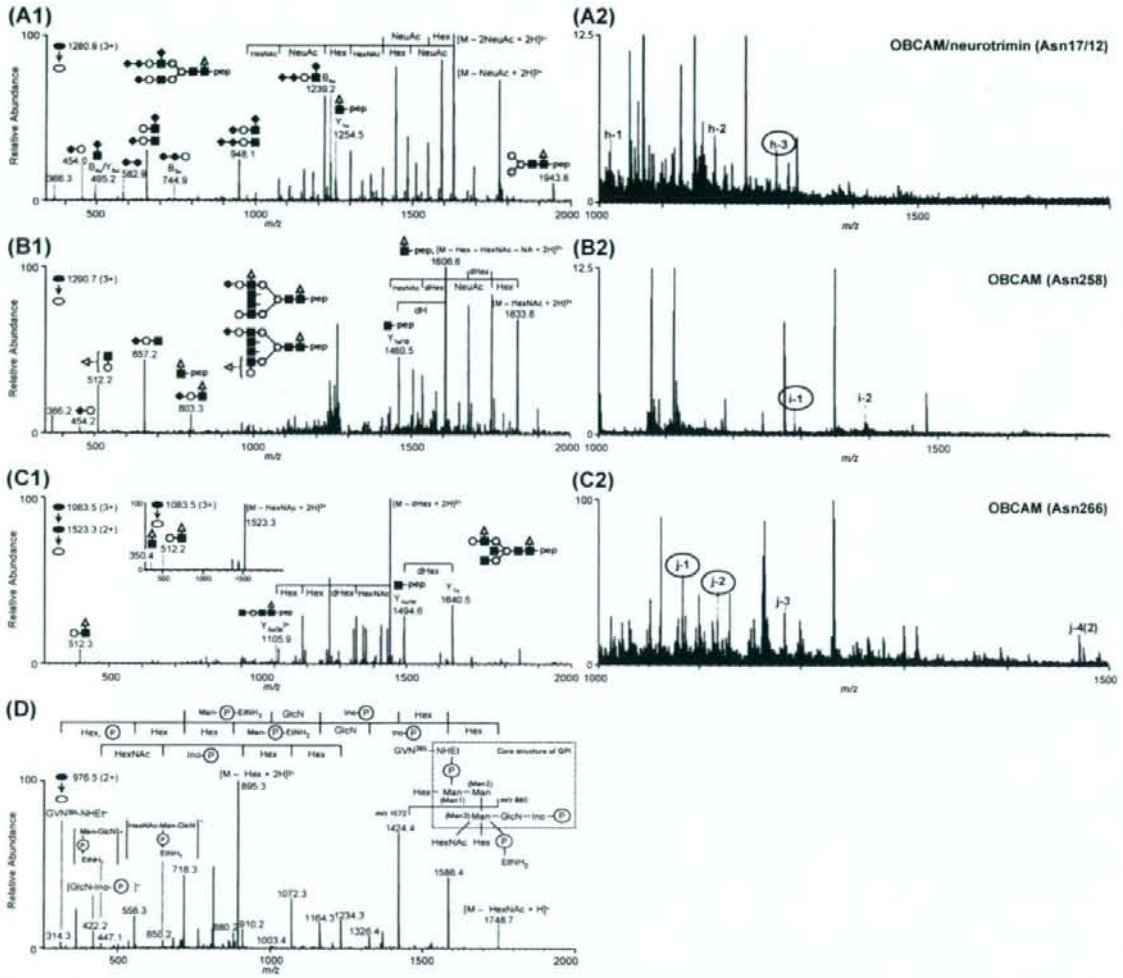

FIGURE 6: MS spectra of OBCAM glycopeptides. (A1) MS/MS spectra of glycopeptide AMDN[17]VTVR; elution position, 2; precursor ion, $[M + 3H]^{3+}$ (*m/z* 1280.9). (A2) Integrated mass spectrum obtained from position 2. (B1) MS/MS spectrum of glycopeptide ISTLTFFN[258]VSE; elution position, 25; precursor ion, $[M + 3H]^{3+}$ (*m/z* 1290.7). (B2) Integrated mass spectrum at position 25. (C1) MS/MS and MS/MS/MS spectra of glycopeptide YGN[266]YTCVATNK; elution position, 7; precursor ion, $[M + 3H]^{3+}$ (*m/z* 1083.5). (C2) Integrated mass spectrum at position 7. (D) MS/MS spectrum of GPI-linked GVN[295]; elution position, 26; precursor ion, $[M + 2H]^{2+}$ (*m/z* 976.5). Symbols are as in Figure 9.

glycopeptide containing Asn12 (GTDN[12]ITVR) in neurotrimin is identical to GTDN[17]ITVR in OBCAM, the glycans at Asn12 are estimated to be hybrid and complex types containing disialic acid (panel A2 of Figure 6 and Table 1G). Likewise, the sequence of VAWLN[38]R in neurotrimin is identical to that of VAWLN[38]R in LAMP, and therefore, the linkage of Man-5-9 at Asn38 was inferred from the glycosylation at Asn38 in LAMP (panel A2 of Figure 5 and Table 1A). Although the MS/MS spectra of glycopeptides containing Asn120 were not acquired, glycosylation at Asn120 was confirmed by the identification of GND[120]ISLTCIATGR, GND[120]ISLTCIATGRPE, and GND[120]ISLTCIATGRPEPTVTWR after PNGase F digestion (data not shown). The substitution of Asn184 with a Lys or an Arg residue in neurotrimin was suggested as in case of SD rat by the identification of VTVNYPPYISE, which is a fragment of VN[184]VTVNYPPYISE (data not shown) (*33*).

The MS/MS spectra of glycopeptides containing Asn252, -260, -273, and -289 were located at positions 20, 5, 23, and 26 based on the peptide-related ions, respectively (panels A1−C1 and D of Figure 7). The integrated mass spectrum of the glycopeptides containing Asn252, -260, and -273 are shown in panels A2−C2 of Figure 7, respectively.

(i) Asn252. Panel A1 of Figure 7 shows the representative MS/MS spectra of glycopeptide LTFFN[252]VSE linked by $dHex_2Hex_6HexNAc_4$, acquired at position 20. A $Le^{a/x}$ -modified core-fucosylated and bisected hybrid-type oligosaccharide was deduced from the $Le^{a/x}$-related ions, and $Y_{1\beta/3\alpha/3\beta}{}^{2+}$ and $Y_{1\alpha}$. The majority of the glycans at Asn252 are estimated to be $Le^{a/x}$ or $Le^{b/y}$-modified complex- and hybrid-type oligosaccharides from the molecular ions (peaks k-1−9) in the integrated mass spectrum and their MS/MS spectra (panel A2 of Figure 7 and Table 1K).

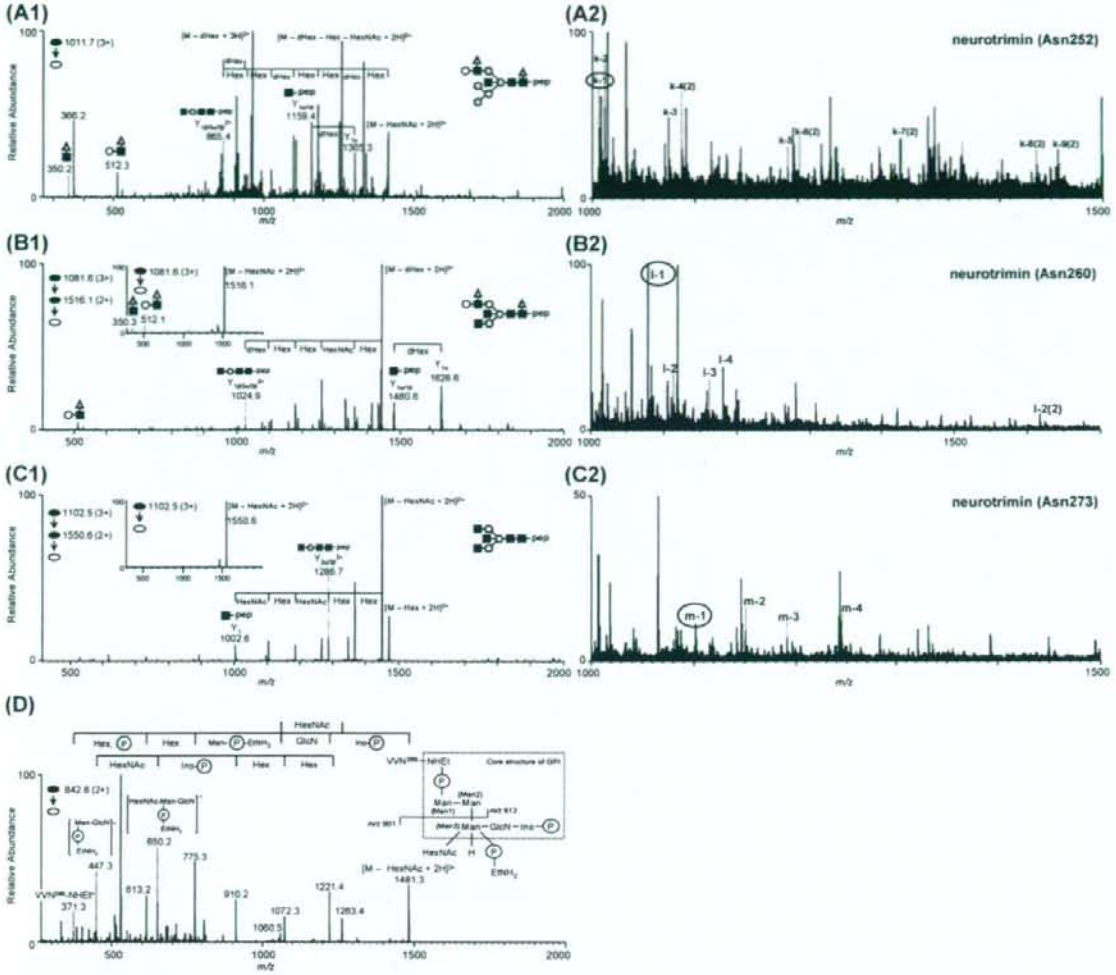

FIGURE 7: MS spectra of neurotrimin glycopeptides. (A1) MS/MS spectra of glycopeptide LTFFN^{252}VSE; elution position, 20; precursor ion, $[M + 3H]^{3+}$ (m/z 1011.7). (A2) Integrated mass spectrum obtained from position 20. (B1) MS/MS and MS/MS/MS spectra of glycopeptide YGN^{260}YTCVASNK; elution position, 5; precursor ion, $[M + 3H]^{3+}$ (m/z 1081.6). (B2) Integrated mass spectrum at position 5. (C1) MS/MS and MS/MS/MS spectra of glycopeptide LGHTN^{273}ASIMLFGPGAVSE; elution position, 23; precursor ion, $[M + 3H]^{3+}$ (m/z 1102.5). (C2) Integrated mass spectrum at position 23. (D) MS/MS spectrum of GPI-linked VNN^{289}; elution position, 26; precursor ion, $[M + 2H]^{2+}$ (m/z 842.8). Symbols are as in Figure 9.

(ii) Asn260. Panel B1 of Figure 7 shows the representative product ion spectra of the glycopeptide eluted at position 5, the peptide portion of which was identified as YGN^{260}YTCVASNK on the basis of the $Y_{1\alpha/1\beta}$ ion in the MS/MS/MS spectrum. The monosaccharide composition ($dHex_2Hex_4HexNAc_5$), the Le$^{a/x}$-related ions in the MS/MS spectrum, and the presence of $Y_{1\beta/3\alpha/3\beta}{}^{2+}$ and $Y_{1\alpha}$ in the MS/MS/MS spectrum revealed the linkage of a Le$^{a/x}$-modified fucosylated and bisected complex-type oligosaccharide to this peptide (inset of panel B1 of Figure 7). The molecular ions in the integrated mass spectrum (peaks I-1−4 in panel B2 of Figure 7) together with the MS/MS spectra of glycosylated HDYGN^{260}YTCVASNK (position 8) suggested that Asn260 was predominantly glycosylated with the Le$^{a/x}$ or Le$^{b/y}$-modified bisected complex- and hybrid-type oligosaccharides and BA-2 (Table 1L).

(iii) Asn273. On the basis of the Y_1 ion and the monoisotopic mass, the glycopeptide eluted at position 23 was assigned to LGHTN^{273}ASIMLFGPGAVSE glycosylated with $Hex_3HexNAc_5$ (panel C1 of Figure 7). Its glycan moiety was characterized as a bisected agalacto-complex-type oligosaccharide based on $Y_{3\alpha/3\beta}{}^{2+}$. Other glycans at Asn273 were assigned to bisected complex- and hybrid-type oligosaccharides (peaks m-1−4 in panel C2 of Figure 7 and Table 1M).

(iv) Asn289. Figure 7D shows one of the MS/MS spectra of GPI-linked VNN^{289}, which was picked out from position 26 on the basis of the peptide-related ion (peptide-NH-Et$^+$, m/z 371.3). Three different MS/MS spectra of GPI-linked VNN^{289} were picked out from position 26 (Figure 4B). From the molecular ions [peaks N1 (m/z 1004), N2 (m/z 924), and N3 (m/z 842)] and their fragments, it was suggested that they contain Hex-Man1 and HexNAc-(Hex-)(NH_2Et-PO_4-)Man3,

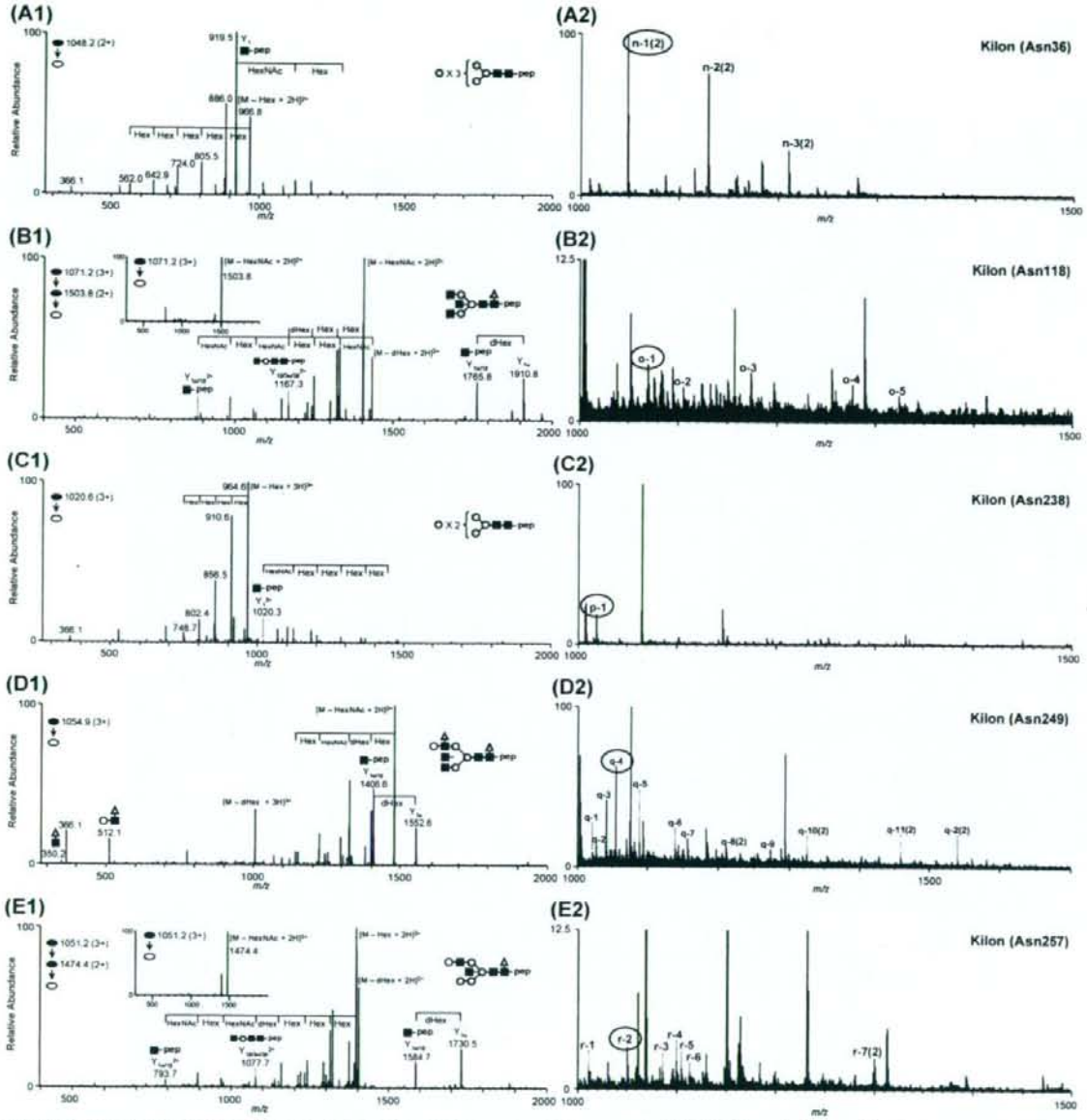

FIGURE 8: MS spectra of Kilon glycopeptides. (A1) MS/MS spectra of glycopeptide GAWLN[36]R; elution position, 3; precursor ion, $[M + 2H]^{2+}$ (m/z 1048.2). (A2) Integrated mass spectrum obtained from position 3. (B1) MS/MS and MS/MS/MS spectra of glycopeptide GTN[118]VTLTCLATGKPE; elution position, 16; precursor ion, $[M + 3H]^{3+}$ (m/z 1071.2). (B2) Integrated mass spectrum at position 16. (C1) MS/MS spectrum of glycopeptide LFNGQQGIIIQN[238]FSTR; elution position, 22; precursor ion, $[M + 3H]^{3+}$ (m/z 1020.6). (C2) Integrated mass spectrum at position 22. (D1) MS/MS spectrum of glycopeptide SILTVTN[249]VTQE; elution position, 17; precursor ion, $[M + 3H]^{3+}$ (m/z 1054.9). (D2) Integrated mass spectrum at position 17. (E1) MS/MS and MS/MS/MS spectra of glycopeptide HFGN[257]YTCVAANK; elution position, 10; precursor ion, $[M + 3H]^{3+}$ (m/z 1051.2). (E2) Integrated mass spectrum at position 10. Symbols are as in Figure 9.

HexNAc-(Hex-)(NH_2Et-PO_4-)Man3, and HexNAc-(NH_2Et-PO_4-)Man3, respectively. The existence of two isomers was suggested in peak N2 by the presence of two different MS/MS spectra at different elution times (Table 2).

Glycosylation Analysis of Kilon. Kilon has six potential N-glycosylation sites at Asn36, -118, -238, -249, -257, and -270. The predicted linkage site of GPI is Gly287. The typical MS/MS spectra and the integrated mass spectra of the glycopeptides containing Asn36, -118, -238, -249, and -257 are shown in panels A1−E1 and A2−E2 of Figure 8, respectively. The MS/MS spectra of the glycopeptide containing both Asn270 and Gly287 could not be picked out from the MS data.

(i) Asn36. Panel A1 of Figure 8 shows one of the MS/MS spectra acquired at position 3. This glycopeptide was identified as GAWLN[36]R with Man-6 based on Y_1 ion and the monosaccharide composition. Other glycans at Asn36 were estimated as Man-5, -7, and -8 from the existence of

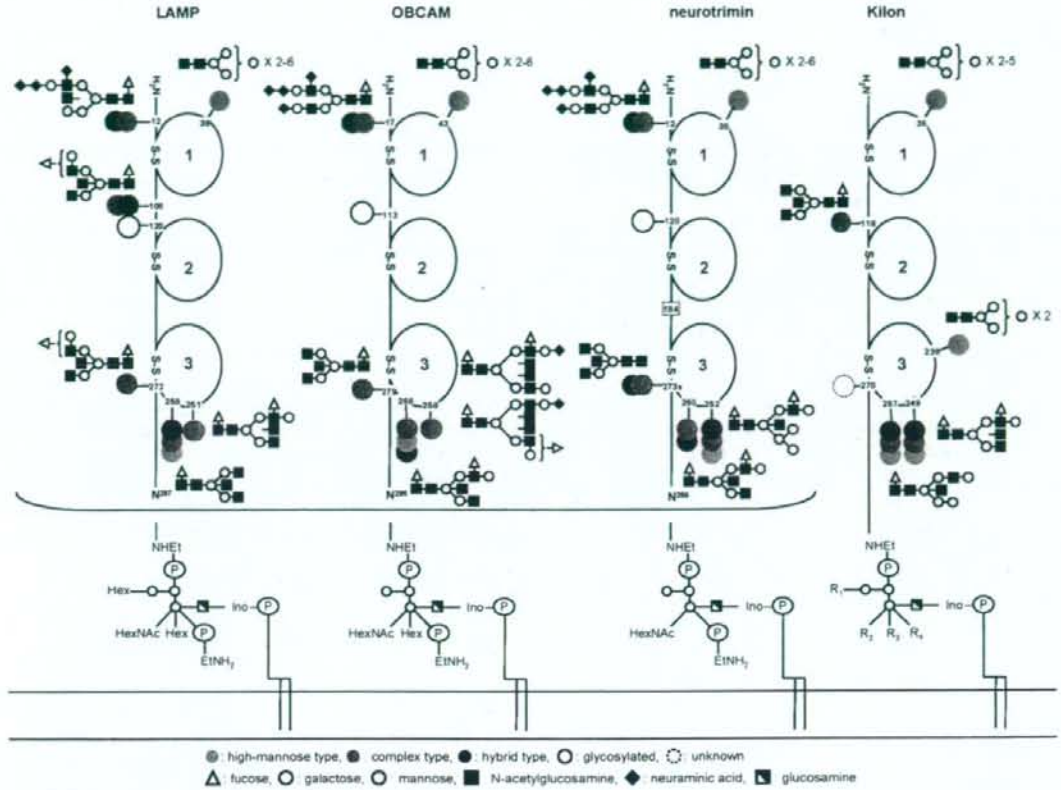

FIGURE 9: Summary of glycosylation of IgLON family proteins.

molecular ions with 81 *m/z* units intervals in the integrated mass spectrum (peaks n-1−3 in panel A2 of Figure 8) (Table 1N).

(ii) Asn118. As shown in panel B1 of Figure 8, the MS/MS/MS spectrum acquired at position 16 contained $Y_{1\alpha/1\beta}$, which suggested that the peptide portion is GTN[118]VTLTCLATGKPE. The linkage of BA-2 was deduced from the monosaccharide composition ($dHex_1Hex_3HexNAc_5$), and $Y_{1\beta/3\alpha/3\beta}{}^{2+}$ and $Y_{1\alpha}$ (inset of panel B1 of Figure 8). Additionally, the linkage of $Le^{a/x}$ or antigen H-modified and/or bisected complex type was suggested by the integrated mass spectrum (peaks o-1−5 in panel B2 of Figure 8 and Table 1O).

(iii) Asn238. The MS/MS spectra of glycopeptides that contain Asn238 were picked out from positions 22 [LFNGQQGIIIQN[238]FSTR (panel C1 of Figure 8)], 21 (RLFNGQQGIIIQN[238]FSTR), and 19 (KRLFNGQQGIII-QN[238]FSTR). These MS/MS spectra and molecular ions appearing in the integrated mass spectrum revealed that the only carbohydrate structure at Asn238 was Man-5 (peak p-1 in panel C2 of Figure 8 and Table 1P). Together with the results of the database search analysis, in which nonglycosylated peptide LFNGQQGIIIQN[238]FSTR was identified, it was suggested that Man-5 was partly attached to Asn238 (Table 1P).

(iv) Asn249. Panel D1 of Figure 8 shows the representative MS/MS spectrum of glycopeptide SILTVTN[249]VTQE at position 17. The carbohydrate structure was characterized as a $Le^{a/x}$-modified and core-fucosylated complex type by the existence of the $Le^{a/x}$-related ions and $Y_{1\alpha}$. The integrated mass spectrum and alternative LC−MS^n with the C30 column (scan ranges of *m/z* 700−2000 and 1000−2000) suggested that Asn249 is glycosylated with $Le^{a/x}$ or antigen H-modified core-fucosylated hybrid- and complex-type oligosaccharides, BA-2, and Man-5 (peaks q-1−11 in panel D2 of Figure 8 and Table 1Q).

(v) Asn257. As shown in panel E1 of Figure 8, one of the glycopeptides eluted at position 10 was identified as HFGN[257]YTCVAANK linked by $dHex_1Hex_5HexNAc_4$ based on $Y_{1\alpha/1\beta}$ ion in the MS/MS/MS spectra and monoisotopic mass. The carbohydrate structure was characterized as a bisected- and core-fucosylated hybrid-type oligosaccharide based on the presence of $Y_{1\beta/3\alpha/3\beta}{}^{2+}$ and $Y_{1\alpha}$ (inset of panel E2 of Figure 8). Other major glycans were estimated as Man-5, $Le^{a/x}$-modified complex- and hybrid-type oligosaccharides, and BA-2 (peaks r-1−7 in panel E2 of Figure 8 and Table 1R).

DISCUSSION

The cell adhesion molecules in the central nervous system play an essential role in the differentiation of neuronal cells and formation of neural circuits. Although glycosylation on the cell adhesion molecules is known to regulate cell−cell interactions (*2*−*4*), their carbohydrate structures remain unknown due to the difficulty with respect to their isolation and the limited sample amounts. The glycans in the IgLON family proteins are considered to be implicated in the

formation of neural circuits, including migration of neuronal cells, axonal guidance, and fasciculation. However, the high degree of homology of their amino acid sequences makes it difficult to isolate them from each other and to analyze their carbohydrate structures in detail.

In this study, we performed a site-specific glycosylation analysis of LAMP, OBCAM, neurotrimin, and Kilon simultaneously using SDS−PAGE and LC−MS^n. Enriched GPI-linked proteins were separated by SDS−PAGE, and four target proteins were extracted from a gel piece together with other contaminating proteins. The protein mixture was digested and analyzed by the C30 and C18-LC−MS^n runs via MS, data-dependent MS in SIM by the FT ICR-MS, and data-dependent MS/MS and MS/MS/MS. A set of MS data consisting of the mass spectrum, the mass spectrum acquired by the FT ICR-MS in SIM mode, the data-dependently acquired MS/MS, and the MS/MS/MS spectra of a glycopeptide was selected from all MS data on the basis of the existence of the oligosaccharide characteristic oxonium ions in the MS/MS spectrum. The carbohydrate structure and peptide sequence were deduced from the carbohydrate-related ions and peptide-related ions in the product ion spectra. The structural assignment of the glycopeptide was confirmed by the accurate mass acquired on the FT ICR-MS. The b- and y-ions arising from the peptide backbone in the MS/MS/MS spectra were also used for the peptide assignment. The carbohydrate heterogeneity at each glycosylation site was characterized by integrating the mass spectra of the glycopeptides which yielded identical peptide-related ions. We successfully determined the site-specific glycosylation in LAMP, OBCAM, neurotrimin, and Kilon with the exception of Asn120 in LAMP, Asn113 in OBCAM, Asn120 in neurotrimin, and Asn270 in Kilon. We also demonstrated the structure of the GPI moiety using LC−MS^n equipped with a GCC. A set of data was picked out from all MS data by using GPI-characteristic ions, and the structure of GPI and the linkage site were deduced from the product ions in the MS/MS spectra. Three different structures are commonly found in LAMP, OBCAM, and neurotrimin.

Figure 9 illustrates the site-specific glycosylation in the four proteins. N-Glycosylation sites near the N-terminus in LAMP, OBCAM, and neurotrimin were commonly occupied with biantennary complex-type and hybrid-type oligosaccharides containing disialic acids. Oligosialic acids and disialic acids, which are found in several glycoproteins, including NCAM, are considered to regulate the cell−cell interaction by changing their degree of polymerization (*6*). Disialic acids at the near N-terminus in LAMP, OBCAM, and neurotrimin might regulate the cell−cell interaction in a manner similar to that of other glycosylated adhesion molecules.

The first domains in IgLON family proteins are commonly glycosylated with Man-5, -6, -7, -8, and -9. The linkage of high-mannose-type oligosaccharides is found in several Ig superfamily proteins, including L1, MAG, and P0 (*3*). Since Horstkorte et al. have reported that L1 binds to NCAM through oligomannosidic carbohydrates in L1 (*34*), the high-mannose-type oligosaccharide in IgLON family proteins could interact with certain biological molecules.

The third domains of all IgLON proteins were highly heterogeneous due to a linkage of diverse oligosaccharides, including BA-2, the $Le^{a/x}$ or $Le^{b/y}$ motif, and Man-5. BA-2, a bisected agalacto-complex type, is known as a brain-specific glycan and is much more abundant in mammalian brains than in other tissues (*35, 36*). Recently, the Na^+/K^+-ATPase $\beta 1$ subunit was identified as a GlcNAc-binding protein in the mouse brain (*37*). The Na^+/K^+-ATPase $\beta 1$ subunit is a potassium-dependent lectin which binds to GlcNAc-terminating oligosaccharides and is involved in neural cell interactions in a trans-binding fashion. A 74 kDa protein was suggested to be the GlcNAc-terminating glycan carrier protein binding to the Na^+/K^+-ATPase $\beta 1$ subunit. The linkage of BA-2 to IgLON family proteins implies that these proteins might be the ligand proteins for the Na^+/K^+-ATPase $\beta 1$ subunit.

Glycosylation in a great number of membrane glycoproteins remains largely unknown. This is mainly because the limited amount of available sample and the low solubility of glycoproteins make their isolation quite difficult. Our strategy, which includes enrichment of the target glycoproteins, separation by SDS−PAGE, and LC−MS^n of digests of a protein mixture, can be applied to the site-specific glycosylation analysis of various membrane glycoproteins.

ACKNOWLEDGMENT

We thank Dr. Masayuki Kubota and Morihiko Yoshida (Thermo Fisher Scientific K.K.) for their technical support.

REFERENCES

1. Walsh, F. S., and Doherty, P. (1997) Neural cell adhesion molecules of the immunoglobulin superfamily: Role in axon growth and guidance. *Annu. Rev. Cell Dev. Biol. 13*, 425–456.
2. Kleene, R., and Schachner, M. (2004) Glycans and neural cell interactions. *Nat. Rev. Neurosci. 5*, 195–208.
3. Krog, L., and Bock, E. (1992) Glycosylation of neural cell adhesion molecules of the immunoglobulin superfamily. *APMIS, Suppl. 27*, 53–70.
4. Schachner, M., and Martini, R. (1995) Glycans and the modulation of neural-recognition molecule function. *Trends Neurosci. 18*, 183–191.
5. Liedtke, S., Geyer, H., Wuhrer, M., Geyer, R., Frank, G., Gerardy-Schahn, R., Zahringer, U., and Schachner, M. (2001) Characterization of N-glycans from mouse brain neural cell adhesion molecule. *Glycobiology 11*, 373–384.
6. Rutishauser, U. (1996) Polysialic acid and the regulation of cell interactions. *Curr. Opin. Cell Biol. 8*, 679–684.
7. Kunemund, V., Jungalwala, F. B., Fischer, G., Chou, D. K., Keilhauer, G., and Schachner, M. (1988) The L2/HNK-1 carbohydrate of neural cell adhesion molecules is involved in cell interactions. *J. Cell Biol. 106*, 213–223.
8. Cho, T. M., Hasegawa, J., Ge, B. L., and Loh, H. H. (1986) Purification to apparent homogeneity of a μ-type opioid receptor from rat brain. *Proc. Natl. Acad. Sci. U.S.A. 83*, 4138–4142.
9. Funatsu, N., Miyata, S., Kumanogoh, H., Shigeta, M., Hamada, K., Endo, Y., Sokawa, Y., and Maekawa, S. (1999) Characterization of a novel rat brain glycosylphosphatidylinositol-anchored protein (Kilon), a member of the IgLON cell adhesion molecule family. *J. Biol. Chem. 274*, 8224–8230.
10. Levitt, P. (1984) A monoclonal antibody to limbic system neurons. *Science 223*, 299–301.
11. Pimenta, A. F., Zhukareva, V., Barbe, M. F., Reinoso, B. S., Grimley, C., Henzel, W., Fischer, I., and Levitt, P. (1995) The limbic system-associated membrane protein is an Ig superfamily member that mediates selective neuronal growth and axon targeting. *Neuron 15*, 287–297.
12. Schofield, P. R., McFarland, K. C., Hayflick, J. S., Wilcox, J. N., Cho, T. M., Roy, S., Lee, N. M., Loh, H. H., and Seeburg, P. H. (1989) Molecular characterization of a new immunoglobulin superfamily protein with potential roles in opioid binding and cell contact. *EMBO J. 8*, 489–495.
13. Struyk, A. F., Canoll, P. D., Wolfgang, M. J., Rosen, C. L., D'Eustachio, P., and Salzer, J. L. (1995) Cloning of neurotrimin

defines a new subfamily of differentially expressed neural cell adhesion molecules. *J. Neurosci. 15*, 2141–2156.
14. Brauer, A. U., Savaskan, N. E., Plaschke, M., Prehn, S., Ninnemann, O., and Nitsch, R. (2000) IG-molecule Kilon shows differential expression pattern from LAMP in the developing and adult rat hippocampus. *Hippocampus 10*, 632–644.
15. Gil, O. D., Zhang, L., Chen, S., Ren, Y. Q., Pimenta, A., Zanazzi, G., Hillman, D., Levitt, P., and Salzer, J. L. (2002) Complementary expression and heterophilic interactions between IgLON family members neurotrimin and LAMP. *J. Neurobiol. 51*, 190–204.
16. Hachisuka, A., Nakajima, O., Yamazaki, T., and Sawada, J. (2000) Developmental expression of opioid-binding cell adhesion molecule (OBCAM) in rat brain. *Brain Res. Dev. Brain Res. 122*, 183–191.
17. Miyata, S., Matsumoto, N., Taguchi, K., Akagi, A., Iino, T., Funatsu, N., and Maekawa, S. (2003) Biochemical and ultrastructural analyses of IgLON cell adhesion molecules, Kilon and OBCAM in the rat brain. *Neuroscience 117*, 645–658.
18. Zacco, A., Cooper, V., Chantler, P. D., Fisher-Hyland, S., Horton, H. L., and Levitt, P. (1990) Isolation, biochemical characterization and ultrastructural analysis of the limbic system-associated membrane protein (LAMP), a protein expressed by neurons comprising functional neural circuits. *J. Neurosci. 10*, 73–90.
19. Hachisuka, A., Yamazaki, T., Sawada, J., and Terao, T. (1996) Characterization and tissue distribution of opioid-binding cell adhesion molecule (OBCAM) using monoclonal antibodies. *Neurochem. Int. 28*, 373–379.
20. Wada, Y., Tajiri, M., and Yoshida, S. (2004) Hydrophilic affinity isolation and MALDI multiple-stage tandem mass spectrometry of glycopeptides for glycoproteomics. *Anal. Chem. 76*, 6560–6565.
21. Wuhrer, M., Hokke, C. H., and Deelder, A. M. (2004) Glycopeptide analysis by matrix-assisted laser desorption/ionization tandem time-of-flight mass spectrometry reveals novel features of horseradish peroxidase glycosylation. *Rapid Commun. Mass Spectrom. 18*, 1741–1748.
22. Satomi, Y., Shimonishi, Y., and Takao, T. (2004) N-Glycosylation at Asn(491) in the Asn-Xaa-Cys motif of human transferrin. *FEBS Lett. 576*, 51–56.
23. Zaia, J. (2004) Mass spectrometry of oligosaccharides. *Mass Spectrom. Rev. 23*, 161–227.
24. Wuhrer, M., Catalina, M. I., Deelder, A. M., and Hokke, C. H. (2007) Glycoproteomics based on tandem mass spectrometry of glycopeptides. *J. Chromatogr., B: Anal. Technol. Biomed. Life Sci 849*, 115–128.
25. Wuhrer, M., Koeleman, C. A., Hokke, C. H., and Deelder, A. M. (2005) Protein glycosylation analyzed by normal-phase nano-liquid chromatography-mass spectrometry of glycopeptides. *Anal. Chem. 77*, 886–894.
26. Harazono, A., Kawasaki, N., Kawanishi, T., and Hayakawa, T. (2005) Site-specific glycosylation analysis of human apolipoprotein B100 using LC/ESI MS/MS. *Glycobiology 15*, 447–462.
27. Sandra, K., Devreese, B., Van Beeumen, J., Stals, I., and Claeyssens, M. (2004) The Q-Trap mass spectrometer, a novel tool in the study of protein glycosylation. *J. Am. Soc. Mass Spectrom. 15*, 413–423.
28. Itoh, S., Kawasaki, N., Harazono, A., Hashii, N., Matsuishi, Y., Kawanishi, T., and Hayakawa, T. (2005) Characterization of a gel-separated unknown glycoprotein by liquid chromatography/multistage tandem mass spectrometry: Analysis of rat brain Thy-1 separated by sodium dodecyl sulfate-polyacrylamide gel electrophoresis. *J. Chromatogr., A 1094*, 105–117.
29. Bordier, C. (1981) Phase separation of integral membrane proteins in Triton X-114 solution. *J. Biol. Chem. 256*, 1604–1607.
30. Lisanti, M. P., Sargiacomo, M., Graeve, L., Saltiel, A. R., and Rodriguez-Boulan, E. (1988) Polarized apical distribution of glycosyl-phosphatidylinositol-anchored proteins in a renal epithelial cell line. *Proc. Natl. Acad. Sci. U.S.A. 85*, 9557–9561.
31. Itoh, S., Kawasaki, N., Ohta, M., and Hayakawa, T. (2002) Structural analysis of a glycoprotein by liquid chromatography-mass spectrometry and liquid chromatography with tandem mass spectrometry. Application to recombinant human thrombomodulin. *J. Chromatogr., A 978*, 141–152.
32. Kikuchi, M., Hatano, N., Yokota, S., Shimozawa, N., Imanaka, T., and Taniguchi, H. (2004) Proteomic analysis of rat liver peroxisome: Presence of peroxisome-specific isozyme of Lon protease. *J. Biol. Chem. 279*, 421–428.
33. Nakajima, O., Hachisuka, A., Takagi, K., Yamazaki, T., Ikebuchi, H., and Sawada, J. (1997) Expression of opioid-binding cell adhesion molecule (OBCAM) and neurotrimin (NTM) in *E. coli* and their reactivity with monoclonal anti-OBCAM antibody. *NeuroReport 8*, 3005–3008.
34. Horstkorte, R., Schachner, M., Magyar, J. P., Vorherr, T., and Schmitz, B. (1993) The fourth immunoglobulin-like domain of NCAM contains a carbohydrate recognition domain for oligomannosidic glycans implicated in association with L1 and neurite outgrowth. *J. Cell Biol. 121*, 1409–1421.
35. Chen, Y. J., Wing, D. R., Guile, G. R., Dwek, R. A., Harvey, D. J., and Zamze, S. (1998) Neutral N-glycans in adult rat brain tissue: Complete characterisation reveals fucosylated hybrid and complex structures. *Eur. J. Biochem. 251*, 691–703.
36. Nakakita, S., Natsuka, S., Ikenaka, K., and Hase, S. (1998) Development-dependent expression of complex-type sugar chains specific to mouse brain. *J. Biochem. 123*, 1164–1168.
37. Kitamura, N., Ikekita, M., Sato, T., Akimoto, Y., Hatanaka, Y., Kawakami, H., Inomata, M., and Furukawa, K. (2005) Mouse Na^+/K^+-ATPase β1-subunit has a K^+-dependent cell adhesion activity for β-GlcNAc-terminating glycans. *Proc. Natl. Acad. Sci. U.S.A. 102*, 2796–2801.

BI8009778

Available online at www.sciencedirect.com
ScienceDirect
Biologicals 36 (2008) 27–36
BIOLOGICALS
www.elsevier.com/locate/biologicals

Prion removal by nanofiltration under different experimental conditions

Mikihiro Yunoki [a,b,*], Hiroyuki Tanaka [b], Takeru Urayama [a,b], Shinji Hattori [b], Masahiro Ohtani [b], Yuji Ohkubo [b], Yoshiyasu Kawabata [b], Yuuki Miyatake [b], Ayako Nanjo [b], Eiji Iwao [c], Masanori Morita [b], Elaine Wilson [d], Christine MacLean [d], Kazuyoshi Ikuta [a]

[a] *Department of Virology, Research Institute for Microbial Diseases, Osaka University, Japan*
[b] *Research & Development Division, Benesis Corporation, Japan*
[c] *Pharmaceutical Research Division, Mitsubishi Pharma Corporation, Japan*
[d] *BioReliance, Invitrogen BioServices, UK*

Received 21 December 2006; revised 11 April 2007; accepted 27 April 2007

Abstract

Manufacturing processes used in the production of biopharmaceutical or biological products should be evaluated for their ability to remove potential contaminants, including TSE agents. In the present study, we have evaluated scrapie prion protein (PrP^{Sc}) removal in the presence of different starting materials, using virus removal filters of different pore sizes. Following 75 nm filtration, PrP^{Sc} was detected in the filtrate by Western blot (WB) analysis when a "super-sonicated" microsomal fraction derived from hamster adapted scrapie strain 263K (263K MF) was used as the spike material. In contrast, no PrP^{Sc} was detected when an untreated 263K MF was used. By using spike materials prepared in a manner designed to optimize the particle size distribution within the preparation, only 15 nm filtration was shown to remove PrP^{Sc} to below the limits of detection of the WB assays used under all the experimental conditions. However, infectious PrP^{Sc} was recovered following 15 nm filtration under one experimental condition. The results obtained suggest that the nature of the spike preparation is an important factor in evaluating the ability of filters to remove prions, and that procedures designed to minimize the particle size distribution of the prion spike, such as the "super-sonication" or detergent treatments described herein, should be used for the preparation of the spike materials.
© 2007 The International Association for Biologicals. Published by Elsevier Ltd. All rights reserved.

Keywords: Prion; Removal; Filter; Clearance study; Spike material

1. Introduction

The transmission of variant Creutzfeldt–Jakob disease (vCJD) through blood transfusion has been of increasing concern, since a fourth possible transmission case was reported [1]. In addition, prions have been detected in the buffy coat separated from the blood of hamsters infected with scrapie, using a biochemical assay (protein misfolding cyclic amplification, or PMCA) [2]. Infectious prions are thought to be the causative agent of the transmissible spongiform encephalopathy (TSE) diseases, which include Creutzfeldt–Jakob disease (CJD), vCJD, and bovine spongiform encephalopathy (BSE). Therefore, to reduce the risk of transmission when raw materials for protein products (such as plasma) are contaminated with infectious prions, measures should be introduced to decrease the prion load, to evaluate the risk to the product, and to introduce prion removal/inactivation step(s) in the manufacturing process, if feasible [3–5]. Unlike viruses, the minimum infectious prion unit does not exist as a single particle. The infectious prion unit is believed to be composed of protein polymers/aggregates, rather than a prion particle. The unusual nature of the prion agent makes it particularly important to

* Corresponding author. Hirakata Research Laboratory, Research & Development Division, Benesis Corporation, 2-25-1 Shodai-Ohtani, Hirakata, Osaka 573-1153, Japan. Tel.: +81 72 850 0100; fax: +81 72 864 2341.
E-mail address: yunoki.mikihiro@mk.m-pharma.co.jp (M. Yunoki).

1045-1056/07/$34.00 © 2007 The International Association for Biologicals. Published by Elsevier Ltd. All rights reserved.
doi:10.1016/j.biologicals.2007.04.005

consider the effect of the prion spike material when evaluating process steps for prion clearance. A rationale for the choice of the spike preparation used for such evaluation studies should be provided [4].

Several prion strains have been used to evaluate manufacturing processes for their ability to remove TSE agents, including hamster scrapie prion protein (PrP^{Sc}, 263K or Sc237), and mouse PrP^{BSE} (301V). In a polyethylene glycol (PEG) fractionation process, hamster PrP^{Sc} and human PrP^{vCJD}, prepared using the same methodology, were reported to behave in a very similar manner [6]. Different prion spike preparations have been used to investigate prion removal, including crude brain homogenate (BH), microsomal fraction (MF), caveolae-like domains (CLDs), and purified PrP^{Sc}. Of these materials, purified PrP^{Sc} was reported to behave differently from the other preparations in an 8% ethanol fractionation step [7]. This result suggests that the methods used to prepare the prion spike material may be a critical factor in prion clearance studies. Furthermore, these reports are useful in providing a rationale for the choice of the prion source and spike preparation used for such evaluation studies [8].

Tateishi et al. reported that sarkosyl influenced the ability of BMM40 filters to remove prions, using BH derived from CJD-infected mice [9]. The presence of sarkosyl was also shown to significantly reduce the capacity of Planova (P)-35N to remove the scrapie agent ME7, while filtration with P-15N resulted in the complete removal of infectivity, to below the limit of detection of the bioassay used, in both the presence and absence of sarkosyl [10]. Van Holten et al. evaluated the capacity of Viresolve 180 membranes (designed for virus removal from proteins of <180 kDa) to remove prions by using BH which was lysolecithin-treated, sonicated, and subsequently passed through a 100 nm filter (SBH), and demonstrated removal of PrP^{Sc} down to the limit of detection of the Western blot assay used. They argued that by using a better defined spike material, where the size of the scrapie particles was limited, the results may be more relevant with respect to the removal of potential TSE infectivity in plasma than previous studies that used a less well-defined BH [11].

Aggregation of the prion protein is a critical parameter when evaluating nanofiltration steps. The actual form of the infectious agent present in plasma in natural infection is not known. In addition, nanofiltration is typically performed late in the downstream processing, after protein purification steps, which may result in removal of larger or aggregated prion forms. Therefore, use of a spike preparation containing large aggregates may result in an over-estimate of the prion removal capacity of a filter. Although the reports described above, and others, have shown excellent prion removal ability for a number of filters, most reports have not described the particle size distribution of the prion protein in the spike preparations used. Therefore, in this study we have investigated the prion removal capacity of P-35N, P-20N and P-15N filters under diverse conditions, considering the particle size distribution of the MF preparations used.

2. Materials and methods

2.1. Preparation of microsomal fraction (MF)

Brains removed from hamsters infected with scrapie strain 263K [12] (originally obtained from the Institute for Animal Health, Edinburgh, UK), were homogenized in phosphate buffered saline (PBS) until homogeneous, to a final concentration of 10% (w/v). The homogenate was clarified by low speed centrifugation, to remove larger cell debris and nuclei, and the supernatant material was then further clarified by centrifugation at 8,000 × *g* for 10 min at 4 °C, before being ultracentrifuged at 141,000 × *g* for 60 min at 4 °C, to concentrate the scrapie fibrils, and small membrane vesicles and fragments. The pelleted material was resuspended in PBS, aliquoted, and stored at −80 °C. This material was designated 263K MF. Prior to use, stocks were thawed at 37 °C, and sonicated 2 × 4 min on ice water (Ultrawave ultrasonic bath model #U100, 130 W 30 kHz, Ultrawave Ltd., Cardiff, UK). Six independent batches of 263K MF were used in this study. These batches are designated 263K MF preparation lots A–F (Tables 1–3). Normal MF, derived from normal (i.e. uninfected) hamster brain material, was also prepared as described above.

Since we were unable to measure the particle size distribution of contaminated materials in our facility, we used normal MF, and investigated changes in the particle size distribution following strong sonication or treatment with detergent. Various concentrations of sarkosyl (*N*-lauroylsarcosine sodium salt, Nacalai Tesque, Inc., Kyoto, Japan), lysolecithin (L-α-lysophosphatidylcholine, Sigma-Aldrich Corp., St. Louis, USA), Triton X-100 (polyethylene glycol mono-*p*-isooctylphenyl ether, Nacalai Tesque, Inc.), TNBP (tri-n-butyl phosphate, Wako Pure Chemical Industries, Ltd., Osaka, Japan), and/or 1% Tween 80 (Nacalai Tesque, Inc.) were added to normal MF. Changes in the particle size distribution were then monitored by dynamic light scattering method using volume-weighted gaussian analysis using a submicrometer particle sizer (NICOMP Type 370, Particle Sizing Systems, Inc., Santa Barbara, USA). To evaluate the effect of strong sonication, normal MF was sonicated using a closed system ultrasonic cell disruptor (Bioruptor UCD-200T, CosmoBio Co. Ltd., Tokyo, Japan) with a resonance chip set in the tube. Sonication was performed for 1 min at 20 kHz, 200 W in a cold water-bath. Ten cycles of sonication were performed, with a 1 min

Table 1
Scrapie infectivity in different 263K MF preparations[a]

	Log_{10} LD_{50}/ml	SE at 95% probability
Non-super-sonicated 263K MF lot C	5.7	0.44
Super-sonicated 263K MF lot C	6.0	0.53
Super-sonicated 263K MF lot D	5.3	0.69
SD-treated, ultracentrifuged, super-sonicated and 220 nm-filtered 263K MF lot C	6.9	0.69

[a] This bioassay study was performed in accordance with GLP regulations.

Table 2
Removal of PrP^{Sc} from PrP^{Sc}-inoculated PBS

	PVDF filter				Planova filter					
	220 nm		100 nm		P-75N (72 ± 2 nm)		P-35N (35 ± 2 nm)		P-15N (15 ± 2 nm)	
Super-sonicated	+	−	+	−	+	−	+	−	+	−
Before filtration	4.2/3.5[a]	3.5/4.2	4.2/3.5	3.5/4.2	4.2/4.2	3.5/4.2	4.2/4.2	3.5/4.2	4.2/4.2	3.5/4.2
Filtered	3.8/3.8	3.1/3.8	3.8/3.1	2.4/3.1	2.4/2.4	<1.0/<1.0	<1.0/<1.0	<1.0/<1.0	<1.0/<1.0	<1.0/<1.0
LRF[b]	0.4/−0.3	0.4/0.4	0.4/0.4	1.1/1.1	1.8/1.8	≥2.5/≥3.2	≥3.2/≥3.2	≥2.5/≥3.2	≥3.2/≥3.2	≥2.5/≥3.2

Data represents total PrP^{Sc} present in samples, expressed as $\log_{10}$ arbitrary units, following Western blot analysis as described for WB1. This study was performed in accordance with GLP regulations.

[a] Two independent batches of 263K MF were used: lot C (left) and lot D (right), respectively.

[b] LRF, log reduction factor = total PrP^{Sc} in input/total PrP^{Sc} in filtrate, expressed as a $\log_{10}$ value.

interval between each sonication treatment. During the treatment cycle, the particle size distribution was monitored. We named this treatment cycle "super-sonication".

Different preparations of 263K MF, treated with various combinations of detergent, ultracentrifugation and/or "super-sonication", were used as the spiking agent in the process evaluation studies, and are described in the relevant methods sections below.

2.2. Detection of PrP^{Sc} by Western blotting (WB)

To determine the relative levels of PrP^{Sc} present in different samples, WB assays were performed. Three slightly different WB methodologies were applied over the course of the studies, all of which are based on detection of the disease-associated, protease-resistant form of the prion protein (PrP^{Sc}), using the monoclonal antibody 3F4 (Signet Laboratories, Inc., Dedham, USA) [13]. WB methods 1 and 2 were developed independently, and use different approaches to calculate the titer of PrP^{Sc}. As these assays were performed as part of GLP studies intended for regulatory submission, the results are presented as reported in these studies.

2.2.1. Method 1 (WB1)

Samples and controls were either tested directly, or first ultracentrifuged at 141,000 × *g* for 60 min at 4 °C, and the pelleted material then resuspended in PBS. Ultracentrifugation was performed to concentrate the PrP^{Sc} present in large volume samples, and to remove soluble proteins or buffer components that might interfere with the WB assay. Samples were digested with proteinase K (Roche Diagnostics, GmbH, Penzberg, Germany) for 60 min at 37 °C. The optimal concentration of proteinase K, to remove any background that could interfere with the detection of PrP^{Sc} and to allow effective recovery of the PrP^{Sc} protein, was previously established for each sample. Digested samples were mixed 1:1 with Laemmli sample buffer (62.5 mM Tris–HCl, pH 6.8, 25% (v/v) glycerol, 2% (w/v) SDS, and 0.01% (w/v) bromophenol blue, BioRad Laboratories Inc., Hercules, USA) containing 5% (v/v) β-mercaptoethanol. After boiling, serial 5-fold dilutions of

Table 3
Removal of PrP^{Sc} from PrP^{Sc}-inoculated plasma preparations[a]

Filter	P-35N (35 ± 2 nm)		P-20N (19 ± 2 nm)		P-15N (15 ± 2 nm)			
Preparation	IVIG	Haptoglobin	IVIG	Haptoglobin	Antithrombin			Thrombin
Spike material	263K sMF[c]	263K sMF[c]	263K sMF[d]	263K dsMF[e]	263K dMF[f]	263K sMF[c]		263K dsMF[e]
MF preparation lot.	C/D	B	E/F	E/F	A/A	B		C/D
Spike ratio	1/100	1/200	1/20	1/200	1/50	1/21		1/20
Detection method[b]	WB1	WB3	WB2	WB2	WB1	WB3	BA	WB1
Before filtration	3.2/2.5	2.4	6.8/6.8	6.7/6.1	3.1/3.1	3.6	+ve	3.7/3.7
Filtered	0.8/0.8	<1.0	4.8/4.3	4.8/4.7	0.0/0.0	<0.8	+ve	<0.2/<0.2
Log reduction factor	2.4/1.7	≥1.4	2.0/2.5	1.9/1.4	≥3.1/≥3.1	≥2.8	NA	≥3.5/≥3.5

Abbreviations used: 263K MF, microsomal fraction derived from hamster adapted scrapie strain 263K; IVIG, intravenous immunoglobulin; 263K sMF, "super-sonicated" 263K MF; WB, Western blotting; 263K dsMF, detergent treated and "super-sonicated" 263K MF; 263K dMF, detergent treated 263K MF; BA, bioassay; +ve, scrapie positive.

[a] Scaled down conditions were designed according to current guidelines. However, in a study using P-35N filter and haptoglobin, clogging of the filter occurred, and the filtration was subsequently terminated.

[b] WB1, WB2, and WB3 mean Western blotting methods 1, 2 and 3, respectively. The studies involving the use of WB1 and WB2 were performed in accordance with GLP regulations; the studies involving the use of WB3 and the qualitative BA shown in this table, were performed as non-GLP studies.

[c] 263K MF was "super-sonicated" then 220 nm-filtered prior to spiking.

[d] 263K MF was ultracentrifuged at 141,000 × *g* for 60 min at 4 °C, resuspended in buffer equivalent to the starting material without protein, "super-sonicated", and 220 nm-filtered prior to spiking.

[e] 263K MF was "SD-treated", ultracentrifuged at 141,000 × *g* for 60 min at 4 °C, resuspended in the starting material (thrombin) or saline (haptoglobin), and "super-sonicated". These materials were 220 nm-filtered prior to spiking.

[f] 263K MF was treated with 0.1% sarkosyl for 30 min at room temperature.